14
Heavy ion collisions

The only practical way of creating and studying hot and dense strongly interacting matter in the laboratory is by colliding heavy nuclei at high energies. Some of the pioneering studies have used nuclear emulsion data of highly energetic cosmic ray events. However, a serious handicap there is the lack of control over the physical beam characteristics. For a few decades now, there has existed a vibrant experimental program seeking to explore the physics of nuclear collisions in different energy regimes and with different combinations of beam and target nuclei. The pioneering experiments at the Lawrence Berkeley National Laboratory (Berkeley, USA) have been followed by several other experimental ventures. It is impossible to enumerate all the facilities, but some important efforts at the high end of the energy spectrum have been pursued at the GSI (Darmstadt, Germany), CERN (Geneva, Switzerland), and at Brookhaven National Laboratory (Upton, USA). The Relativistic Heavy Ion Collider (RHIC) is located at BNL, and the Large Hadron Collider (LHC) has a heavy ion program expected to begin at CERN around 2007. A healthy experimental program in high energy nuclear collisions requires a basis in nucleon–nucleon and nucleon–nucleus collisions. These in fact constitute a crucial category of control experiments for the more complex nucleus–nucleus events. The study of strongly interacting matter at high temperature and density enjoys an active and fruitful collaboration between the experimental and theoretical communities.

In relativistic nuclear collisions, multiple scatterings involving both the primary constituents (the original nucleons) and the secondary particles (mostly created pions) can, in principle, drive the system towards a state of local thermodynamic equilibrium. The reason for this originates in the phenomenology of hadronic collisions. From those studies it is known that, at energies relevant for the applications considered in this chapter,

the large inelastic part of the nucleon–nucleon cross section will cause considerable energy loss of the colliding constituents. This energy loss ultimately translates into the creation of a large number of light mesons, mostly appearing in the central rapidity region, which is midway between the projectile and target fragmentation regions. The identity of the primordial fields first materializing at mid-rapidity (partons or composites) is not completely clear but should depend on the initial energy density. The key issue, however, is the following: because of the large particle multiplicities involved, the relativistic collisions of heavy nuclei will create zones of short mean free paths. This condition will pave the way to the statistical treatment of heavy ion collisions that we shall discuss in this chapter. We have seen that QCD predicts a transition from hot hadronic matter to quark–gluon plasma, provided that the energy density is large enough. We also will review some of the probes that have been proposed to study hot and dense systems and to determine whether a new state of matter has been created.

14.1 Bjorken model

Fermi was the first to apply statistical techniques to hadronic particle production in p–p collisions [1]. Shortly thereafter, the first application of relativistic hydrodynamics to a strongly–interacting system was made by Landau [2]. The power, elegance, and simplicity of hydrodynamics is essentially contained in the statement that the entire system can be described by a few macroscopic thermodynamic fields. The conditions necessary for this to be so are that any modification of the state of the system is reflected instantaneously in the fields. Quantitatively, this statement identifies any relaxation time as shorter than any other time scale in the system under scrutiny. Local thermal equilibrium is therefore assumed. We also assume that the net baryon number and electric charge are zero. Not only does this simplify the analysis but it is a very good approximation in high energy collisions because of the large number of particles produced.

We have already seen, in Chapter 6, that the energy–momentum tensor may be written as

$$T^{\mu\nu} = -Pg^{\mu\nu} + (\epsilon + P)u^\mu u^\nu \tag{14.1}$$

where P is the pressure, ϵ is the energy density, and $u^\mu = (\gamma, \gamma\mathbf{v})$ is the local flow velocity relative to some fixed reference frame. In a frame in which the fluid is locally at rest, $u^\mu = (1, 0, 0, 0)$, $T^{00} = \epsilon$, $T^{ij} = P\delta_{ij}$, and $T^{i0} = 0$. The conservation of energy and momentum is expressed as

$$\partial_\mu T^{\mu\nu} = 0 \tag{14.2}$$

This vector equation, (14.2), represents a set of four scalar equations. However, there are five unknown quantities: the three independent components of the flow velocity u^μ (the normalization condition $u^2 = 1$ defines three independent and one dependent component), the energy density, and the pressure. To close this system, another equation must be supplied, and this is the equation of state. This set of equations can always be solved numerically. However, their solution is a complicated task in three spatial dimensions unless simplifying assumptions are placed on the symmetry of the system. There is a wide body of literature devoted to the techniques used in numerical simulations using relativistic hydrodynamics.

Insight can be gained by considering some simple limits. Motivated by empirical observations, Bjorken [3] was led to explore the consequences of the existence of a central plateau structure in the inclusive particle production as a function of the spacetime rapidity y, defined as

$$y = \frac{1}{2} \ln \left(\frac{t + z}{t - z} \right) \tag{14.3}$$

where the z-axis is oriented along the beam direction. Theoretically, the existence of this plateau implies that the initial conditions, viewed at the same proper time after the beginning of the nuclear collision, are invariant with respect to Lorentz transformations along the longitudinal (or beam) direction.

Another assumption of the Bjorken scenario is that essentially all the baryon number is carried by the receding Lorentz-contracted nuclei that have just collided. The produced particles then occupy the central rapidity region and the high multiplicity will ensure rapid thermalization followed by hydrodynamic evolution. At this point it is appropriate to note that this approach is really a conceptual idealization. In actual practice, the manifest success of the hydrodynamic model in relativistic nuclear collisions at RHIC energies suggests a very early thermalization, even though the microscopic mechanisms that would drive it currently remain unclear.

In keeping with Bjorken's line of thought, we shall be interested in the early stages of the hydrodynamic development of the central collision of high-energy nuclei. There the flow can be assumed one dimensional, owing largely to the initial symmetry of the colliding system. At slightly later times, larger than those associated with the size of the nucleus ($t > 1.2A^{1/3}$ fm/c), the rarefaction wave coming in from the nuclear surface will be fully formed and a three-dimensional expansion will set in. Therefore, the early solution will be independent of the rapidity, and nothing in the time evolution will spoil this symmetry. One may write the general solutions as $\epsilon(\tau)$, $P(\tau)$, $T(\tau)$, $u^\mu(\tau)$, with proper time $\tau = \sqrt{t^2 - z^2}$. Solving

for t and z in terms of τ and y yields

$$t = \tau \cosh y \qquad z = \tau \sinh y \tag{14.4}$$

Then

$$u^\mu = \frac{dx^\mu}{d\tau} = (\cosh y, 0, 0, \sinh \tau) \tag{14.5}$$

and indeed, $u^\mu u_\mu = 1$. One may then write

$$u^\mu \frac{\partial \tau}{\partial x^\mu} = u^0 \frac{\partial \tau}{\partial t} + u^3 \frac{\partial \tau}{\partial z} = \cosh^2 y - \sinh^2 y \equiv 1$$

and

$$\frac{\partial \tau}{\partial x^\mu} = \frac{x_\mu}{\tau} \tag{14.6}$$

The equation for the conservation of energy and momentum is

$$\partial_\mu T^{\mu\nu} = \frac{\partial T^{\mu\nu}}{\partial x^\mu} = \frac{\partial(\epsilon + P)}{\partial \tau} \frac{\partial \tau}{\partial x^\mu} u^\mu u^\nu + (\epsilon + P) \frac{\partial u^\mu}{\partial x^\mu} u^\nu$$

$$+ (\epsilon + P) u^\mu \frac{\partial u^\nu}{\partial x^\mu} - g^{\mu\nu} \frac{\partial P}{\partial \tau} \frac{\partial \tau}{\partial x^\mu} = 0 \tag{14.7}$$

With the help of (14.6), this reduces to

$$\frac{\partial \epsilon}{\partial \tau} + \frac{\epsilon + P}{\tau} = 0 \tag{14.8}$$

Defining an entropy density $s = S/V = (\epsilon + P)/T$ and using the facts that $u^\mu \partial/\partial x^\mu = d/d\tau$ and that at constant volume $d\epsilon = T ds$, we may rewrite the above equation as

$$\frac{ds}{d\tau} + \frac{s}{\tau} = 0 \tag{14.9}$$

the solution of which clearly satisfies

$$\frac{s(\tau)}{s(\tau_0)} = \frac{\tau_0}{\tau} \tag{14.10}$$

Also implied by (14.9) is

$$\frac{\partial (s u^\mu)}{\partial x^\mu} = \partial_\mu s^\mu = 0 \tag{14.11}$$

Entropy is therefore a conserved quantity. Furthermore, since a volume element in this geometry is $dV = d^2x_\perp \tau dy$, (14.10) also means that the entropy per unit rapidity, dS/dy, is a constant with respect to proper time.

Let us now study the time evolution implicit in the formalism we have just written down. We start by considering the case of a first-order phase

transition. Our pragmatic approach will be to describe the quark–gluon plasma as a noninteracting gas of eight massless gluons and two flavors (*u*, *d*) of massless quarks. Note that massive strange quarks could also be included self-consistently. A bag constant B [4] is used to simulate the effect of confinement in the hadron phase, which is described as a noninteracting gas of massless pions. Thus the pressure, energy density, and entropy density in each of the two phases are

$$P_q = 37aT^4 - B \qquad \epsilon_q = 111aT^4 + B \qquad s_q = 148aT^3$$
$$P_h = 3aT^4 \qquad \epsilon_h = 9aT^4 \qquad s_h = 12aT^3 \tag{14.12}$$

where $a = \pi^2/90$. The critical temperature is determined by pressure balance to be

$$T_c = \left(\frac{B}{34a}\right)^{1/4} \tag{14.13}$$

Thus B may be eliminated in favor of T_c. The latent heat necessary to liberate the color degrees of freedom is $4B$.

We may write

$$\frac{d\epsilon}{d\tau} = \frac{d\epsilon}{dP}\frac{dP}{dT}\frac{dT}{d\tau} = -\frac{sT}{\tau} \tag{14.14}$$

where (14.8) has been used. Note that $dP = sdT$ at constant volume. The sound velocity is

$$v_s^2 = \frac{dP}{d\epsilon} \tag{14.15}$$

Putting all this together,

$$\frac{1}{T}\frac{dT}{d\tau} = -\frac{v_s^2}{\tau} \tag{14.16}$$

which yields

$$T = T_0 \left(\frac{\tau_0}{\tau}\right)^{v_s^2} \tag{14.17}$$

For the equations of state in (14.12), $v_s^2 = 1/3$ except at T_c. At T_c it is necessary to specify in addition the volume fraction f of the quark–gluon phase. The entropy density is

$$s(f, T_c) = s_q(T_c)f + s_h(T_c)(1 - f) \tag{14.18}$$

and similarly for the energy density.

We assume now that the nucleus–nucleus collision produces a quark–gluon plasma with initial entropy density $s_0 > s_q(T_c)$. The temperature evolves according to (14.17) until T drops to T_c. This occurs in the proper time interval $\tau_0 < \tau \leq \tau_1 = (T_0/T_c)^3\tau_0$. Assuming that the nucleation of

the hadron phase is fast, the system then enters the mixed phase. In the mixed phase the entropy density decreases, not by decreasing T but by converting quark–gluon plasma to hadron matter at lower entropy density but still at T_c. The fraction $f(\tau)$ is easily derived to be

$$f(\tau) = \frac{1}{r-1}\left(r\frac{\tau_1}{\tau} - 1\right) \qquad (14.19)$$

where $r = 37/3$ is the ratio of number of degrees of freedom in the two phases. Thus $1 > f > 0$ for $\tau_1 < \tau < \tau_2 = r\tau_1$. The mixed phase terminates at τ_2 whereupon the temperature begins to fall again according to

$$T(\tau) = T_c\left(\frac{\tau_2}{\tau}\right)^{1/3} \qquad (14.20)$$

for $\tau > \tau_2$. The expansion continues until the pions can no longer maintain thermal contact. One can take this as a final breakup temperature T_f, also called the freezeout temperature. In totally dynamical simulations of the nuclear collision this sharp cutoff is avoided.

In the case $s_q(T_c) > s_0 > s_h(T_c)$ we assume that the matter is initially formed in the mixed phase, with volume fraction f_0 determined by

$$s = s_q(T_c)f_0 + s_h(T_c)(1 - f_0) \qquad (14.21)$$

It follows that

$$f(\tau) = \frac{1}{r-1}\left\{[1 + (r-1)f_0]\frac{\tau_0}{\tau} - 1\right\} \qquad (14.22)$$

The system evolves in the mixed phase until $\tau_2 = [1 + (r-1)f_0]\tau_0$. The evolution then follows (14.17) in the hadron phase.

Let us now suppose that the equation of state leads to a second-order phase transition. We parametrize the effective number of massless bosonic degrees of freedom in each of the two phases as

$$N_h(T) = 3 + be^{(T-T_c)/d} \qquad N_q(T) = 37 - ce^{(T-T_c)/d} \qquad (14.23)$$

It is straightforward to verify that this leads to a second-order phase transition (P and s continuous but ds/dT discontinuous) provided that $b + c = 34$, $b > 0$, $b \neq 17$. Consistently with our discussion of the Weinberg sum rules in Chapter 12, let us require the ρ and a_1 mesons to become effectively massless at T_c. Then $b = 18$. Setting $c = 16$ produces 21 massless bosonic degrees of freedom at T_c, corresponding to the up and down quarks. The missing 16 degrees of freedom correspond to the eight massless gluons, which may not be readily available at T_c. The entropy is $4aT^3N(T)$, and the evolution can easily be charted using (14.10). The parameter d controls the degree-of-freedom conversion rate. For the sake of illustration we choose $d = 0.034\,T_c$.
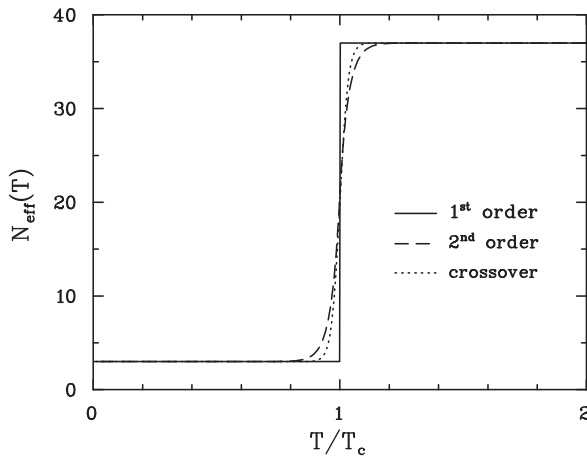
Fig. 14.1. The number of degrees of freedom as a function of the temperature for equations of state producing phase transitions of the first order (solid line) and of the second order (broken line). The effect of a rapid crossover (dotted line) is also shown.

A rapid-crossover scenario is produced by the parametrization

$$N(T) = 20 + 17 \tanh\left(\frac{T - T_{\rm c}}{d}\right) \tag{14.24}$$

The transitions from one set of degrees of freedom to another are shown in Figure 14.1, for the different schemes we have considered: a first-order phase transition, a second-order transition, and a rapid crossover. Similarly, the temperature evolution associated with each of these is shown in Figure 14.2.

Another powerful feature of the Bjorken model is the particle production. Since the entropy density of a gas of massless pions is proportional to the pion number density, it follows that the entropy can be determined by measuring the charged-particle multiplicity $N_{\rm ch}$. Considering a head-on collision of equal-mass nuclei, one finds approximately

$$\frac{dN_{\rm ch}}{dy} = \left(f_0 + \frac{1 - f_0}{r}\right) 3\pi R^2 \tau_0 T_0^3 \tag{14.25}$$

where R is the nuclear radius, $f_0 = 0$ if $T_0 < T_{\rm c}$, $0 \leq f_0 \leq 1$ if $T_0 = T_{\rm c}$, and $f_0 = 1$ if $T_0 > T_{\rm c}$. Those arguments are not significantly altered even if the rather large latent heat is shrunk to zero so that the first-order phase transition turns into a second-order one, or even if there is no proper phase transition at all. The essential requirement is that the number of degrees of freedom should increase by a factor r in a small temperature interval $\Delta T \approx d$. The conservation of entropy density enables one to relate
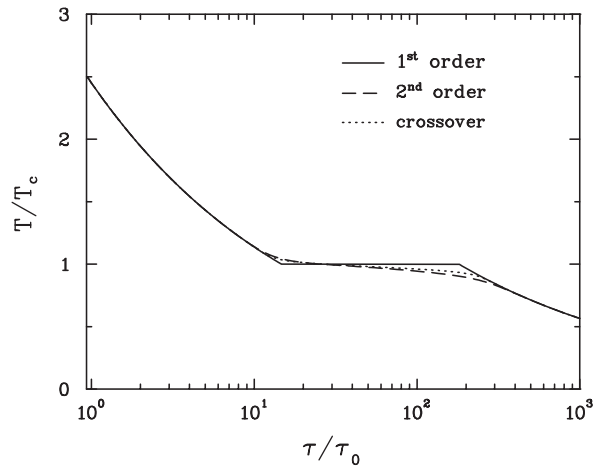
Fig. 14.2. The temperature evolution in the Bjorken model. Note that the plateau in T starts and ends at $\tau = \tau_1$ and τ_2, respectively. See the text for details.

measurements in the final state to parameters that determine the initial conditions for thermal equilibrium and hydrodynamic flow.

In this section, we have used a simple dynamical model for ultrarelativistic nucleus–nucleus collisions, and simple parametrizations of the equation of state to give a flavor of this branch of high-energy nuclear physics. For more sophisticated discussions, the reader is referred to the literature cited at the end of the chapter.

14.2 The statistical model of particle production

As mentioned previously, Fermi's seminal paper was instrumental to the development of statistical techniques for particle production in strongly interacting systems [1]. Fermi's original application was to proton–proton collisions. Our discussion will concentrate on nucleus–nucleus collisions, where the applicability of the model is arguably maximal, but the statistical model has even been applied in the case of e^+e^- collisions [5].

If we assume that the approach to equilibrium can be modeled by a transport equation of the Boltzmann type for the phase-space density $f(x, p)$, we may write

$$\left(\frac{p^\mu}{m} \frac{\partial}{\partial x^\mu} + F^\mu \frac{\partial}{\partial p^\mu} \right) f(x, p) = C[f] \tag{14.26}$$

where F^μ is a generalized force term and $C[f]$ is a collision term that ensures entropy growth. At equilibrium, detailed balance makes the right-hand side of this equation vanish, and thermal distributions functions are recovered. In fact, in high-energy nuclear collisions a statistical approach is natural, as the high multiplicity will provide a physical environment

appropriate for realization of equipartition. Specifically, $\lambda \sim 1/\sigma n$, where σ is a total cross-section, λ is a mean free path, and $n \sim \int d^3p\, f(x,p)$. Thus as the multiplicities increase, the mean free path will decrease. Furthermore, the relevance of statistical arguments should improve in high-temperature environments, owing to the same arguments.

The fundamental quantity that regulates the thermal composition of particle species is the partition function. We will work in the grand canonical ensemble. We have already encountered this quantity in Chapter 1; it is given by $Z = \operatorname{Tr} \hat{\rho}$, where $\hat{\rho}$, the statistical density matrix, is given by (1.1). In a system that we are modeling as a gas of relativistic hadrons (stable and unstable), the quantum numbers we choose to be conserved are electric charge, baryon number, and strangeness. The grand canonical partition function can then be written as a sum of partition functions for individual hadrons and resonances:

$$\ln Z(V, T, \mu_Q, \mu_B, \mu_S) = \sum_i \ln Z_i(V, T, \mu_Q, \mu_B, \mu_S) \qquad (14.27)$$

where

$$\ln Z_i(V, T, \mu_Q, \mu_B, \mu_S) = \pm (2s_i + 1)\frac{V}{2\pi^2} \int_0^\infty dp\, p^2 \ln\left[1 \pm \lambda_i \exp(-\beta \omega_i)\right]$$
$$(14.28)$$

The $+$ or $-$ sign is for fermions or bosons, $2s_i + 1$ is the spin degeneracy factor, $\omega_i = \sqrt{p^2 + m_i^2}$, $\beta = 1/T$, and the fugacity is

$$\lambda_i(T, \mu_Q, \mu_B, \mu_S) = \exp\left[\beta(\mu_Q Q_i + \mu_B B_i + \mu_S S_i)\right] \qquad (14.29)$$

The coordinate-space density of species i is then

$$n_i(T, \mu_Q, \mu_B, \mu_S) = \frac{N_i}{V} = (2s_i + 1)\frac{T}{2\pi^2} \sum_{\ell=1}^\infty \frac{(\pm 1)^{\ell+1}}{\ell} \lambda_i^\ell m_i^2 K_2(\ell \beta m_i)$$
$$(14.30)$$

where $K_2(x)$ is a modified Bessel function. In actual comparisons with experiment, it is especially important to account for resonances decaying into lighter hadrons; then we get a net number

$$N_i^{\text{net}}(T, \mu) = N_i(T, \mu) + \sum_k N_k(T, \mu) B_{k \to i + X} \qquad (14.31)$$

where $B_{k \to i + X}$ is the branching ratio for the decay $k \to i + X$. At high temperatures (around and above the pion mass) the yield of the light mesons is indeed dominated by feed-down from the higher-lying resonances.

In practical applications to measured particle numbers and, especially, ratios, the temperature T and the baryon chemical potential μ_B are the

two main parameters of the model. Note that there is no quantum number associated with the conservation of meson number, unlike baryons. Also, overall strangeness conservation fixes μ_S. Note that this would actually be rigorously true if measurements covered all the phase space, so that all fragments were measured. For measurements performed at mid-rapidity, however, the strangeness entering one region in rapidity is approximately canceled by that leaving. Therefore, even in experiments with a limited phase-space coverage, the strangeness chemical potential can be taken to vanish. In addition, charge conservation requirements have a small influence at RHIC energies and above. Finally, the volume V drops out in analyses of particle number ratios. It can actually be fixed by measuring the total pion multiplicity and requiring agreement between the theoretical expression and the empirical value.

Putting these ingredients together, one may further assume chemical equilibrium and thus verify how far this assumption will hold. Chemical equilibrium implies that if $c \rightleftharpoons a + b$ then $\mu_c = \mu_a + \mu_b$. Therefore, the chemical potential of a given resonance is fixed by its decay systematics and can be written in terms of μ_B. In the final analysis, decay cascades (where several generations of particle decays contribute) are also included. Also of practical concern is whether to use only data at mid-rapidity or data that is integrated over the full phase space. A popular and pragmatic choice is to restrict the analysis to a slice at mid-rapidity centered at zero with a total width of 2 units of rapidity [6]. From CERN experiments, the ratios of particle abundances were fitted at fixed-target bombarding energies of 40 and 158 GeV per nucleon, for collisions of Pb on Pb. At RHIC energies ($\sqrt{s} = 130$ and 200 GeV in the nucleon–nucleon center-of-mass frame), Au + Au collisions were analyzed. At 40 GeV per nucleon, 11 particle ratios were included in the fit while that number was 24 at 158 GeV per nucleon. The lower RHIC energy included 13 species, while the higher energy included five particle ratios; these numbers are continuously updated as the experimental analyses continue. Weak-decay systematics are extremely important: those species that are unstable against the weak interaction will eventually decay and their products will be measured by the experimental detectors. The goodness of fit was evaluated via the minimization of

$$\chi^2 = \sum_i \frac{\left(R_i^{\text{expt}} - R_i^{\text{model}}\right)^2}{\sigma_i^2} \tag{14.32}$$

where R_i is the fraction of particles of species i in the total number of particles of all species and σ_i is its experimental uncertainty. The set of (T, μ_B) values that minimize the above relation is plotted in Figure 14.3. The values of χ^2 attained are about 1 per degree of freedom [6].
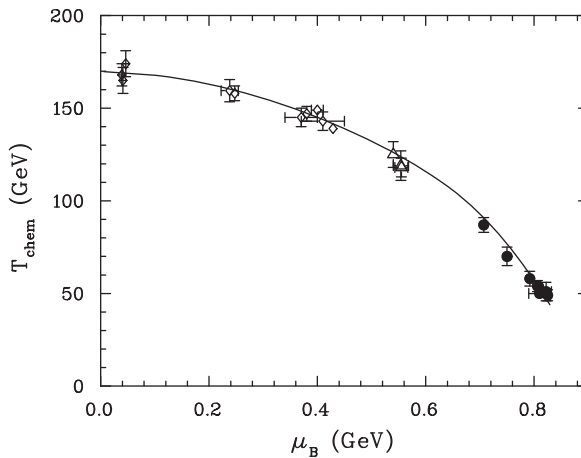
Fig. 14.3. The chemical freezeout temperature against baryon chemical potential as extracted from several fits to measured particle ratios at different energies. The solid line is a curve for which the average energy per hadron $\langle E \rangle / \langle N \rangle = 1$ GeV [7]. The data have been collected from experiments performed at the GSI [8], the AGS at BNL [9], CERN [10, 6], and RHIC [11].

There have been efforts [12] to improve the fits to hadron-yield ratios by invoking a departure from chemical equilibrium and looking for evidence of this deviation in the data. For example, the density of pions is parametrized by generalizing the thermal distribution function to

$$\frac{N_\pi}{V} = 3 \int \frac{d^3p}{(2\pi)^3} \frac{1}{\gamma_\pi^{-1} e^{\omega_\pi/T} - 1} \tag{14.33}$$

where γ_π is a parameter that regulates the absolute chemical equilibrium and is therefore unity in that limit. Values of $\gamma_\pi \neq 1$ would constitute, in this interpretation, a signature of nonequilibrium. We will not pursue this further here, but it is a topic of current investigation.

The fitted values from Figure 14.3 can be reconciled with a global picture that emerged from years of heavy ion phenomenology at CERN's SPS, which we now very briefly summarize. The intuitive picture is as follows. The nuclear system is first heated and compressed. This is followed by a phase of decompression where both the temperature and the density drop. Note here the use of the word temperature, which stems again from years of phenomenological analysis. Two freezeout temperatures may be identified. As the hot, interacting system cools, it eventually breaks apart and its constituents begin free-streaming towards the detectors to be measured individually. A criterion for this to happen is that the mean free path, as defined earlier by the inverse of the product of density and cross section, becomes comparable with the spatial dimensions of the

system:

$$\lambda \sim \frac{1}{n\sigma} \sim R \qquad (14.34)$$

The particle population will be dominated by pions, as they are the lightest species. Some insight on the behavior of the system may then be had by considering chiral perturbation theory. For temperatures below the pion mass, the elastic cross section essentially saturates the total cross section: the inelastic channels manifest themselves at higher powers of the chiral expansion [13]. This means that number-changing interactions will cease before purely elastic interactions do, as the system expands and cools. Another way of thinking about this is related to the fact that inelastic reactions have energy thresholds, whereas elastic interactions do not. Therefore, there will exist a region where $T_{\mathrm{kin}} < T < T_{\mathrm{chem}}$. Here T_{kin} is the kinetic freezeout temperature (where transverse-momentum spectra cease to evolve) and T_{chem} is the temperature below which the particle numbers do not change.

The fact that the curve corresponding to an average energy per particle of 1 GeV traces the path laid out by the thermal-model fit is very suggestive of a critical phenomenon. However, numerical simulations of relativistic nuclear collisions have correlated the energy per particle value of 1 GeV with the onset of inelastic thresholds [14], at least at beam energies that correspond to those spanned in the experimental fits shown in Figure 14.3. It is very suggestive that the low-μ_B chemical freezeout temperatures found in the thermal analysis of experimental nucleus–nucleus data are consistent with the critical temperature extracted from the lattice simulation of QCD, as mentioned in Section 10.5. This would be the case if the chemical composition of the hadrons being measured were established during the hadronization of the quark–gluon plasma. Note also the similarity between Figures 14.3 and 10.9. Although very suggestive, these connections remain the source of much current research.

14.3 The emission of electromagnetic radiation

In theoretical studies of hot and dense strongly interacting systems, electromagnetic radiation constitutes a class of penetrating probes. This is essentially a reflection of the near absence of final-state interactions for photons (real and virtual) that are produced in relativistic nuclear collisions. More quantitatively, at scales relevant for hadronic phenomenology, $\alpha/\alpha_{\mathrm{s}} \sim 0.002 \ll 1$. This means that electromagnetic radiation, once created, will leave the system unscathed. In line with the rest of this chapter, we assume that nuclear collisions at high energies form a thermalized system. As mentioned previously, this assertion receives considerable

empirical support. We will now proceed to derive the rate of emission of electromagnetic radiation from a thermal, strongly interacting, medium. As in any hadronic collision, there will always be emission of electromagnetic radiation from the very first interactions, those involving cold matter. In nucleon–nucleus and in nucleus–nucleus events, this primordial photon and lepton pair emission is usually treated (up to aspects like the Cronin effect, which we do not discuss here) as an additive superposition of nucleon–nucleon contributions, calculated using the techniques of perturbative QCD. The details of this are outside the scope of this book.

Consider generic hadronic states $|i\rangle$ and $|f\rangle$ and a transition between them that involves the absorption or emission of a photon with four-momentum $k^\mu = (\omega, \mathbf{k})$ and polarization ϵ^μ. To make things more definite we shall concentrate on the case of real photons here, and extend our analysis to lepton pair production later. The transition rate between the two states is

$$R_{fi} = \frac{|S_{fi}|^2}{tV} \tag{14.35}$$

tV being the proper four-volume. To leading order in the interaction Hamiltonian (or equivalently, in the one-photon approximation), the S-matrix element is

$$S_{fi} = \langle f| \int d^4x \hat{J}_\mu(x) A^\mu(x)|i\rangle \tag{14.36}$$

$\hat{J}_\mu(x)$ being the hadronic electromagnetic current operator. Considering a free vector field

$$A^\mu(x) = \frac{\epsilon^\mu}{\sqrt{2\omega V}} \left(e^{ik \cdot x} + e^{-ik \cdot x} \right) \tag{14.37}$$

and, invoking translation invariance for the matrix element

$$\langle f|\hat{J}_\mu(x)|i\rangle = e^{i(p_f - p_i) \cdot x} \langle f|\hat{J}_\mu(0)|i\rangle$$

one may write

$$R_{fi} = -\frac{g^{\mu\nu}}{2\omega V}(2\pi)^4 \left[\delta(p_i + k - p_f) + \delta(p_i - k - p_f) \right]$$
$$\times \langle f|\hat{J}_\mu(0)|i\rangle\langle i|\hat{J}_\nu(0)|f\rangle \tag{14.38}$$

One delta function corresponds to the absorption process and the other to emission. The differential thermal emission rate is obtained by keeping the appropriate delta function, summing over final states, and averaging over initial states with a Boltzmann weight $e^{-\beta\hat{K}_i}/Z$, where $Z = \sum_i e^{-\beta\hat{K}_i}$,

and $\hat{K} = \hat{H} - \mu \hat{N}$:

$$\frac{d^3R}{d^3k} = -\frac{g^{\mu\nu}}{2\omega V}\frac{V}{(2\pi)^3}\frac{1}{Z}\sum_i \mathrm{e}^{-\beta\hat{K}_i}\sum_f (2\pi)^4\delta(p_i - p_f - k)$$
$$\times\langle j|\hat{J}_\mu(0)|i\rangle\langle i|\hat{J}_\nu(0)|f\rangle \tag{14.39}$$

Defining, as in Section 6.2, spectral functions associated respectively with absorption and emission,

$$f_{\mu\nu}^\pm(k) = \pm\frac{1}{Z}\sum_{i,f}\mathrm{e}^{-\beta\hat{K}_i}(2\pi)^3\delta(p_i - p_f \pm k)$$
$$\times\langle f|\hat{J}_\mu(0)|i\rangle\langle i|\hat{J}_\nu(0)|f\rangle \tag{14.40}$$

one may use the identity relating them, $f_{\mu\nu}^+(k) = -\mathrm{e}^{\beta\omega}f_{\mu\nu}^-(k)$, to write

$$\omega\frac{d^3R}{d^3k} = \frac{g^{\mu\nu}}{(2\pi)^3}\,\pi f_{\mu\nu}^- \tag{14.41}$$

Note that the symbol used here (f) is different from that used in Chapter 6 (ρ), to make clear the fact that here the correlation functions involve the current operator. One relates the current–current correlators to those involving the fields through the equation of motion $\partial^\mu\partial_\mu A_\nu(x) = J_\nu(x)$, written here in the Feynman gauge. Doing this, and using the fact that the spectral density $\rho_{\mu\nu}^{\mathrm{n}}(k)$ is proportional to the imaginary part of the retarded propagator, (6.33), one obtains

$$\omega\frac{d^3R}{d^3k} = -\frac{g^{\mu\nu}}{(2\pi)^3}\,\mathrm{Im}\,\Pi_{\mu\nu}^{\prime\mathrm{R}}(\omega, \mathbf{k}) \tag{14.42}$$

Here the finite-temperature retarded improper self-energy, $\Pi_{\mu\nu}^{\prime\mathrm{R}}$, is defined through the appropriate Schwinger–Dyson equation, $D = D^0 - D^0\Pi'D^0$. Therefore, to leading order in the electromagnetic interaction but to all orders in the strong interaction,

$$\omega\frac{d^3R}{d^3k} = -\frac{g^{\mu\nu}}{(2\pi)^3}\,\mathrm{Im}\,\Pi_{\mu\nu}^{\mathrm{R}}(\omega, \mathbf{k}) \tag{14.43}$$

where $\Pi_{\mu\nu}^{\mathrm{R}}$ is the finite-temperature retarded photon self-energy.

Repeating this derivation, but for a virtual photon that converts to a lepton pair, we are led to

$$E_+E_-\frac{d^6R}{d^3p_+\,d^3p_-} = \frac{2e^2}{(2\pi)^6}\frac{1}{k^4}\left[p_+^\mu p_-^\nu + p_+^\nu p_-^\mu - g^{\mu\nu}\left(p_+\cdot p_- + m_\ell^2\right)\right]$$
$$\times\Pi_{\mu\nu}^{\mathrm{R}}(\omega, \mathbf{k})\frac{1}{\mathrm{e}^{\beta\omega} - 1} \tag{14.44}$$

where the invariant mass of the virtual photon is $M^2 = k^2 = (p_+ + p_-)^2$, p_+ and p_- are the momenta of the lepton pair components, and m_ℓ is the lepton mass.

14.4 Photon production in high-energy heavy ion collisions

The formation and observation of quark–gluon plasma in ultrarelativistic collisions between heavy nuclei is an important goal of modern nuclear physics. Among the proposed probes of the plasma are the directly produced real photons [15–21]. Microscopically, these could come from the annihilation process $q\bar{q} \to g\gamma$ and from the QCD Compton process $qg \to q\gamma$, $\bar{q}g \to \bar{q}\gamma$. These photons interact only electromagnetically, unlike pions, and so their mean free paths are typically much larger than the transverse size of the region of hot matter created in any nuclear collision. As a result, high-energy photons produced in the interior of the plasma usually pass through the surrounding matter without interacting, carrying information directly from wherever they were formed to the detector. This makes them an interesting object of study to both theorists and experimenters.

Here we concern ourselves with the following questions. What is the spectral emissivity of quark–gluon plasma? What is the spectral emissivity of hot hadronic matter? How do they compare at the same temperature? These are important questions. Suppose we put hadron gas in one box and quark–gluon plasma in another and maintain them at the same temperature T. Can we tell which box contains the quark–gluon plasma by looking through a small window and measuring the photon spectrum? If we wait long enough the answer is clearly no: even if we do not put any photons into the boxes at the beginning, the matter will eventually come to equilibrium under the electromagnetic interactions; to a good approximation the final photon distribution will be just the Planck distribution at temperature T. Fortunately, in conditions more appropriate to a nuclear collision the answer is yes. A closer analog to a nuclear collision is to make the boxes smaller than the photon mean free path and to make the walls transparent to photons, so that the photons always escape and the photon distribution stays far from equilibrium. The spectral emissivity then directly reflects the dynamics of real photon-producing reactions in the matter, which may be different for the two phases. The thermal production rates in the two phases are important in another sense. Suppose that quark–gluon plasma is formed in a collision. It will expand and eventually hadronize in a first- or second-order phase transition or rapid crossover. The hadrons themselves may maintain local thermal equilibrium for a while, also producing photons. The total yield is a sum of the yields from both phases. To make the method clear, we shall mainly
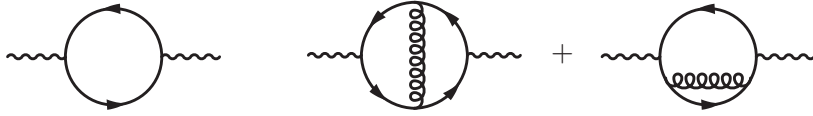
Fig. 14.4. One- and two-loop contributions to the photon self-energy in QCD.

concentrate here on the radiation from the partonic phase of QCD, and follow the treatment in [21].

In an expansion in diagram topologies, the one- and two-loop contributions to $\Pi_{\mu\nu}$ are shown in Figure 14.4. The imaginary part is obtained by cutting the diagrams. Cutting the one-loop diagram gives zero when the photon is on the mass shell since $q\bar{q} \to \gamma$ has no phase space. Certain cuts of the two-loop diagrams give order-g^2 corrections to the nonexistent reaction $q\bar{q} \to \gamma$, while other cuts correspond to the reactions $q\bar{q} \to g\gamma$, $qg \to q\gamma$ and $\bar{q}g \to \bar{q}\gamma$. Let $\mathcal{M}_i$ represent the amplitude for one of these. The contribution to the rate in relativistic kinetic theory for a photon-producing reaction $1 + 2 \to 3 + \gamma$ is

$$
R_i = \mathcal{N} \int \frac{d^3 p_1}{2E_1(2\pi)^3} \frac{d^3 p_2}{2E_2(2\pi)^3} f_1(E_1) f_2(E_2)(2\pi)^4 \delta(p_1^\mu + p_2^\mu - p_3^\mu - p^\mu)
$$

$$
\times |\mathcal{M}_i|^2 \frac{d^3 p_3}{2E_3(2\pi)^3} \frac{d^3 p}{2E(2\pi)^3} [1 \pm f_3(E_3)] \tag{14.45}
$$

where $\mathcal{N}$ is a degeneracy factor, the f's are the Fermi–Dirac or Bose–Einstein distribution functions as appropriate, and there is either a Bose-enhancement or a Pauli-suppression of the strongly interacting particle in the final state. (Another example of the connection between the imaginary part of the finite-temperature retarded self-energy and relativistic kinetic theory can be found in Section 16.6.)

This rate can be simplified. Define $s = (p_1 + p_2)^2$ and $t = (p_1 - p)^2$. Insert integrations over s and t with a delta function for each of these identities. This is a natural thing to do because the invariant amplitude depends only on these two variables. Converting the total rate to a differential one, all but four of the integrations can be done without approximation:

$$
E \frac{d^3 R_i}{d^3 p} = \frac{\mathcal{N}}{(2\pi)^7} \frac{1}{16E} \int ds\, dt \; |\mathcal{M}_i(s,t)|^2 \int dE_1\, dE_2\, f_1(E_1) f_2(E_2)
$$

$$
\times [1 \pm f_3(E_1 + E_2 - E)] \theta(E_1 + E_2 - E)(aE_1^2 + bE_1 + c)^{-1/2} \tag{14.46}
$$

where

$$a = -(s+t)^2$$
$$b = 2(s+t)(Es - E_2 t) \tag{14.47}$$
$$c = st(s+t) - (Es + E_2 t)^2$$

At present we are interested in the case where the photon energy is large, $E_1 + E_2 > E \gg T$. In this limit it is a good approximation to make the replacement

$$f_1(E_1) f_2(E_2) \to e^{-(E_1 + E_2)/T} \tag{14.48}$$

Even though E_1 or E_2 separately need not be large, phase space is unfavorable for it. This approximation can be checked numerically (see Exercise 14.4). Then the integrals over E_1 and E_2 can be done, with the relatively simple result

$$E \frac{d^3 R_i}{d^3 p} = \frac{\mathcal{N}}{(2\pi)^6} \frac{T}{32E} e^{-E/T} \int \frac{ds}{s} \ln(1 \pm e^{-s/4ET})^{\pm 1} \int dt \, |\mathcal{M}_i(s,t)|^2 \tag{14.49}$$

The upper sign is to be taken when particle 3 is a fermion, the lower sign when it is a boson.

For massless particles the amplitude is related to the differential cross section by

$$\frac{d\sigma}{dt} = \frac{|\mathcal{M}|^2}{16\pi s^2} \tag{14.50}$$

For the annihilation diagram,

$$\frac{d\sigma}{dt} = \frac{8\pi \alpha \alpha_s}{9s^2} \frac{u^2 + t^2}{ut} \tag{14.51}$$

where u and t are Mandelstam variables, and $\mathcal{N} = 20$ when summing over the up and down quarks. For the Compton reaction,

$$\frac{d\sigma}{dt} = \frac{-\pi \alpha \alpha_s}{3s^2} \frac{u^2 + s^2}{us} \tag{14.52}$$

and $\mathcal{N} = 320/3$. The integral over t just gives the total cross section. But the total cross section involving the exchange of a massless particle is infinite: the differential cross sections have a pole at t and/or $u = 0$. Many-body effects are necessary to screen this divergence. We will show how this works. For now we delete the region of phase space causing the divergence. We integrate over

$$-s + k_c^2 \le t \le -k_c^2$$
$$2k_c^2 \le s < \infty \tag{14.53}$$

where k_{c} is an infrared cutoff and $T^2 \gg k_{\mathrm{c}}^2 > 0$. This way of regulating the divergence treats u and t symmetrically and maintains the identity $s + t + u = 0$ that is appropriate for all massless particles.

In the limit $k_{\mathrm{c}}^2 \to 0$ we find

$$E\frac{d^3R}{d^3p}^{\mathrm{Compton}} = \frac{5}{9}\frac{\alpha\alpha_s}{6\pi^2}T^2\mathrm{e}^{-E/T}\left[\ln\left(\frac{4ET}{k_{\mathrm{c}}^2}\right) + C_{\mathrm{F}}\right] \quad (14.54)$$

$$E\frac{d^3R}{d^3p}^{\mathrm{annihilation}} = \frac{5}{9}\frac{\alpha\alpha_s}{3\pi^2}T^2\mathrm{e}^{-E/T}\left[\ln\left(\frac{4ET}{k_{\mathrm{c}}^2}\right) + C_{\mathrm{B}}\right] \quad (14.55)$$

where

$$C_{\mathrm{F}} = \frac{1}{2} - \gamma_{\mathrm{E}} + \frac{12}{\pi^2}\sum_{n=2}^{\infty}\frac{(-1)^n}{n^2}\ln n$$
$$= 0.0460\ldots \quad (14.56)$$

$$C_{\mathrm{B}} = -1 - \gamma_{\mathrm{E}} - \frac{6}{\pi^2}\sum_{n=2}^{\infty}\frac{1}{n^2}\ln n$$
$$= -2.1472\ldots \quad (14.57)$$

and γ_{E} is Euler's constant. These expressions use the full Fermi–Dirac or Bose–Einstein distribution functions in the final state. Although $E \gg T$, it is not necessarily the case that $E_3 \gg T$. Taking this into account, one gets slightly different results if one uses the Boltzmann distribution in the final state instead:

$$E\frac{d^3R}{d^3p}^{\mathrm{Compton}} = \frac{5}{9}\frac{2\alpha\alpha_{\mathrm{s}}}{\pi^4}T^2\mathrm{e}^{-E/T}\left[\ln\left(\frac{4ET}{k_{\mathrm{c}^2}}\right) + \frac{1}{2} - \gamma_{\mathrm{E}}\right] \quad (14.58)$$

$$E\frac{d^3R}{d^3p}^{\mathrm{annihilation}} = \frac{5}{9}\frac{2\alpha\alpha_{\mathrm{s}}}{\pi^4}T^2\mathrm{e}^{-E/T}\left[\ln\left(\frac{4ET}{k_{\mathrm{c}}^2}\right) - 1 - \gamma_{\mathrm{E}}\right] \quad (14.59)$$

Corrections to these formulae vanish in the limit $k_{\mathrm{c}} \to 0$.

The essential factors in these rates are easy to understand. There is a factor $5/9$ from the sum of the squares of the electric charges of the u and d quarks, a factor $\alpha\alpha_{\mathrm{s}}$ coming from the topological structure of the diagrams, a factor T^2 from phase space, which gives the overall dimension to the rate, the ubiquitous Boltzmann factor $\mathrm{e}^{-E/T}$ for photons of energy E, and a logarithm due to the infrared behavior.

The infrared divergence in the photon production rate discussed above is caused by a diverging differential cross section when the momentum transfer goes to zero. Often, long-range forces can be screened by
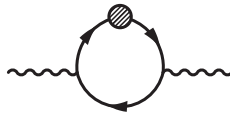
Fig. 14.5. HTL-corrected photon self-energy, in QCD.

many-body effects at finite temperature. In fact, we have already seen concrete examples of this mechanism in Chapter 9. From the hard thermal loops (HTL) analysis, we know that a propagator must be dressed if the momentum flowing through it is soft, on a scale set by the temperature T. For the present application we would begin by replacing the bare propagators and vertices in the one-loop diagram of Figure 14.4 by effective propagators and vertices. The reason is that the propagation of soft momenta is connected with infrared divergences in loops; if we do not dress these propagators we get infinite answers, so the corrections due to the dressing of the propagators are also infinite and therefore necessary. Thus, the results with soft propagators dressed are really the lowest-order finite results. In our case it is necessary to dress one of the quark propagators because our results diverge otherwise. It is not necessary to dress both, nor is it necessary to dress either of the vertices, because these produce only finite corrections that are of higher order in g. We are thus led to evaluate the diagram shown in Figure 14.5. Some insight can be gained by expanding the diagram as a power series in g^2. The zeroth-order term reproduces the one-loop diagram of Figure 14.4. The order-g^2 term reproduces one of the two-loop diagrams of Figure 14.4, with the recognition that the quark self-energy is not the exact one-loop self-energy but is approximated by its high-temperature limit. Clearly this is a summation of an infinite set of diagrams that is purposely designed to regulate infrared problems of the type encountered here.

Starting with Figure 14.5, and summing over u and d quarks, we find

$$\Pi^{\mu\nu}(p) = -6 \times \frac{5}{9}e^2 T \sum_{k_0} \int \frac{d^3k}{(2\pi)^3} \operatorname{Tr}\left[\mathcal{G}^*(k)\gamma^\mu \mathcal{G}(p-k)\gamma^\nu\right] \qquad (14.60)$$

where

$$\mathcal{G}^*(k) = \mathcal{G}^*_+(k)\frac{\gamma_0 - \mathbf{k}\cdot\boldsymbol{\gamma}}{2} + \mathcal{G}^*_-(k)\frac{\gamma_0 + \mathbf{k}\cdot\boldsymbol{\gamma}}{2} \qquad (14.61)$$

is the dressed propagator for a quark with four-momentum k, already encountered in Section 9.4, and

$$\mathcal{G}(q) = g_+(q)\frac{\gamma_0 - \mathbf{q}\cdot\boldsymbol{\gamma}}{2} + g_-(q)\frac{\gamma_0 + \mathbf{q}\cdot\boldsymbol{\gamma}}{2} \qquad (14.62)$$

is the bare propagator for a quark with four-momentum $q = p - k$. The propagator $\mathcal{G}^*(k)$ was defined in (9.37), and

$$g_\pm(q) = (-q_0 \pm \mathbf{q})^{-1} \tag{14.63}$$

Using these expressions for the quark propagators, and evaluating the traces, we obtain

$$\Pi_\mu^{\mathrm{R},\mu}(p) = \frac{20}{3}e^2 T \sum_{k_0} \int \frac{d^3k}{(2\pi)^3} \left\{ \mathcal{G}_+^*(k) \left[g_+(q)\left(1 - \mathbf{k}\cdot\mathbf{q}\right) + g_-(q)\left(1 + \mathbf{k}\cdot\mathbf{q}\right) \right] \right.$$
$$\left. + \mathcal{G}_-^*(k) \left[g_+(q)\left(1 + \mathbf{k}\cdot\mathbf{q}\right) + g_-(q)\left(1 - \mathbf{k}\cdot\mathbf{q}\right) \right] \right\} \tag{14.64}$$

That the self-energy is retarded means that p_0 has a small positive imaginary part, as is appropriate in linear response analysis.

We then follow Braaten, Pisarski, and Yuan [22] in computing the imaginary part in the following elegant way:

$$\operatorname{Im} T \sum_{k_0} F_1(k_0)\, F_2(p_0 - k_0)$$
$$= \frac{1}{2i}\ \operatorname{Disc}\ T \sum_{k_0} F_1(k_0)\, F_2(p_0 - k_0)$$
$$= \pi(1 - \mathrm{e}^{E/T}) \int_{-\infty}^{+\infty} d\omega \int_{-\infty}^{+\infty} d\omega'\, N_\mathrm{F}(\omega)\, N_\mathrm{F}(\omega')$$
$$\times \delta(E - \omega - \omega')\, \rho_1(\omega)\, \rho_2(\omega') \tag{14.65}$$

Here N_F is the Fermi–Dirac occupation number and ρ_1 and ρ_2 are the spectral densities for the two chosen functions F_1 and F_2. Specifically, these are related by

$$F(k_0) = \int_{-\infty}^{+\infty} \frac{d\omega}{\omega - k_0 - i\epsilon}\, \rho(\omega) \tag{14.66}$$

We need the spectral density functions $\rho_\pm^*$ and $r_\pm$ for the dressed and bare propagators, respectively. The latter can be obtained in a straightforward fashion, and the former were given in Chapter 9. Putting this information together we obtain

$$\operatorname{Im} \Pi_\mu^{\mathrm{R},\mu} = -\frac{20\pi}{3}e^2(\mathrm{e}^{E/T} - 1) \int \frac{d^3k}{(2\pi)^3} \int_{-\infty}^{+\infty} d\omega \int_{-\infty}^{+\infty} d\omega'\, \delta(E - \omega - \omega')$$
$$\times\ N_\mathrm{F}(\omega) N_\mathrm{F}(\omega') \left[(1 + \mathbf{q}\cdot\mathbf{k})(\rho_+^* r_- + \rho_-^* r_+) \right.$$
$$\left. + (1 - \mathbf{q}\cdot\mathbf{k})(\rho_+^* r_+ + \rho_-^* r_-) \right] \tag{14.67}$$

with $r_\pm(\omega', \mathbf{q}) = \delta(\omega' \mp |\mathbf{q}|)$. In these expressions ρ_+^* and ρ_-^* (9.39) are evaluated at $(\omega, \mathbf{k})$.

In the kinetic theory calculation we were forced to put a cutoff k_c^2 on the four-momentum transfer t (and on u) to avoid an infrared divergence. This cutoff removes only the small region of phase space left out by (14.53). Anything else must necessarily be higher order in g. Inspection of Figure 14.4 shows that the exchanged quark must be dressed and must satisfy

$$- k_c^2 \leq \omega^2 - \mathbf{k}^2 \leq 0. \tag{14.68}$$

This means that the delta functions (representing poles) in the spectral densities do not contribute to this order, but only the functions $\beta_\pm$ (representing branch cuts); see (9.40).

The energy-conserving delta function, together with the mass-shell delta functions of $r_\pm$, can be used to evaluate the integral over ω' and the integral over the angle between $\mathbf{k}$ and $\mathbf{q}$ in (14.67). Then, making use of the inequalities $E \gg T$ and $0 \leq \mathbf{k}^2 - \omega^2 \leq k_c^2 \ll T^2$, we get

$$\mathrm{Im}\,\Pi_\mu^{\mathrm{R},\mu} = -\frac{5e^2}{6\pi} \left(\mathrm{e}^{E/T} - 1 \right) \mathrm{e}^{-E/T}$$
$$\times \int_0^{k_c} d|\mathbf{k}| \int_{-|\mathbf{k}|}^{|\mathbf{k}|} d\omega \left[(|\mathbf{k}| - \omega)\beta_+(\omega, \mathbf{k}) + (|\mathbf{k}| + \omega)\beta_-(\omega, \mathbf{k}) \right]$$

$$\tag{14.69}$$

The integral involving β_- is the same as the integral involving β_+, so we only need to determine the latter and multiply by 2. Furthermore it is convenient to make the change of variables $|\mathbf{k}| = \tau \cosh \eta$ and $\omega = \tau \sinh \eta$. Then we have for the above double integral

$$2 \int_{-\infty}^{+\infty} d\eta \int_0^{k_c} \tau \, d\tau \, (|\mathbf{k}| - \omega)\beta_+(\omega, \mathbf{k})$$
$$= \frac{m_q^2}{4} \int_{-\infty}^{+\infty} \frac{d\eta}{\cosh^2\eta} \left\{ \ln \left(\frac{(\Theta + y_c \cosh^2\eta)^2 + 1}{\Theta^2 + 1} \right) \right.$$
$$\left. - 2\Theta \left[\tan^{-1}(\Theta + y_c \cosh^2\eta) - \tan^{-1}(\Theta) \right] \right\} \tag{14.70}$$

where

$$\Theta = \frac{2}{\pi} \frac{Q_0(\sinh \eta) - Q_1(\sinh \eta)}{1 - \tanh \eta} \tag{14.71}$$

and

$$y_c = \frac{2}{\pi} \frac{k_c^2}{m_q^2} \tag{14.72}$$

The quantities $Q_0(z)$ and $Q_1(z)$ are Legendre functions.

We still have some freedom in choosing the cutoff k_c. Since g is supposed to be perturbatively small for this whole analysis to make sense let us

choose k_c to lie somewhere in the interval

$$m_q \ll k_c \ll T \tag{14.73}$$

Then we are allowed to take the limit $y_c \gg 1$ in (14.70). Doing so, and dropping terms that vanish in the limit $y_c \to \infty$, we find that the right-hand side becomes

$$m_q^2 \ln\left(\frac{k_c^2}{m_q^2}\right) + \frac{m_q^2}{4} \int_{-\infty}^{\infty} \frac{d\eta}{\cosh^2\eta} \left[\ln\left(\frac{4}{\pi^2} \frac{\cosh^4\eta}{\Theta^2 + 1}\right) - 2\Theta\left(\frac{\pi}{2} - \tan^{-1}\Theta\right)\right] \tag{14.74}$$

This remaining integral is a pure number and is evaluated as $-4\ln 2$.

Now we have all the items we need in order to write down the contribution to the rate coming from the infrared-sensitive (IR) part of phase space:

$$E\frac{d^3 R^{IR}}{d^3 p} = \frac{5}{9}\frac{\alpha\alpha_s}{2\pi^2} T^2 e^{-E/T} \ln\left(\frac{k_c^2}{2m_q^2}\right) \tag{14.75}$$

where

$$2m_q^2 = \frac{g^2 T^2}{3} \tag{14.76}$$

Adding the contributions from both the hard momentum transfers, (14.54) and (14.55), and the soft momentum transfers, (14.75), we get the net rate

$$E\frac{d^3 R}{d^3 p} = \frac{5}{9}\frac{\alpha\alpha_s}{2\pi^2} T^2 e^{-E/T} \ln\left(\frac{2.912}{g^2}\frac{E}{T}\right) \tag{14.77}$$

This is independent of the cutoff k_c! The HTL resummation method works beautifully to screen the infrared divergence. (Inclusion of the exact Bose–Einstein and Fermi–Dirac distributions in the initial state instead of the Boltzmann limit (14.48) leads to a replacement of the numerical factor 2.912 in the logarithm by 3.739. See Exercise 14.4.)

It is apparent that our asymptotic formula breaks down when $E \le g^2 T/2.9$ because the logarithm goes negative. For photon energies that are small on a scale set by the the temperature, a complete calculation should include bremsstrahlung processes. Also, the effective cutoff was determined under the assumption that the photon energy was large. If it is not, then all propagators and vertices in Figure 14.5 must be dressed.

The rate for photon emission described above was computed by taking the imaginary part of Figure 14.5. In a Feynman diagram representation, the HTL correction induces a thermal mass which screens the singularity that would appear when the intermediate-quark propagator goes on-shell. Moving on to a higher topology in the number of loops and taking the imaginary part gives contributions like those of Figure 14.6. These
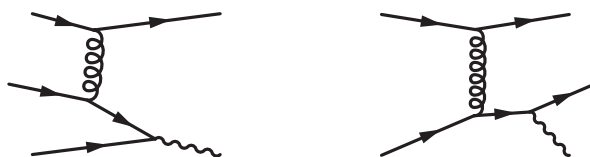
Fig. 14.6. Two photon-producing processes that appear to be of higher order in α_s than the Compton and annihilation contributions.
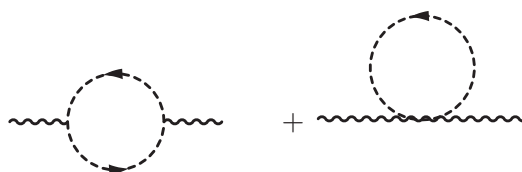

Fig. 14.7. The two Feynman diagrams that contribute to the ρ self-energy. The wavy lines are a neutral ρ, whereas the broken lines represent charged pions.

bremsstrahlung and pair-annihilation plus scattering contributions to the photon emission are superficially of higher order in α_s (they appear to be $\mathcal{O}(\alpha_s^2)$) than the ones we have discussed previously [23]. If the virtuality of the off-shell quark going into the vertex where the photon is being emitted is very small, there is an enhancement in the net thermal emission rate. This can be seen in the prefactor: $\alpha_s^2 T^2/m_q^2 \sim \alpha_s$. Those diagrams, naively of higher order in the strong coupling, contribute parametrically at the same order as the previous ones for low energy photons! The resolution of this apparent paradox was provided by a systematic identification of all processes contributing, to the leading order in α_s, to photon and lepton pair production [24].

For the evaluation of the emissivity of hot matter in the confined, hadronic sector, calculations have mainly followed the techniques outlined in this section. In particular, most practitioners have used relativistic kinetic theory and considered the contributing processes, such as $\pi\rho \rightarrow \pi\gamma$ and $\pi\pi \rightarrow \rho\gamma$, channel by channel. This closely parallels the first part of this section, where the annihilation and Compton contributions to the photon spectrum in hot QCD were considered. Many authors have contributed to this line of study. An early analysis was that given in reference [21]. A recent assessment of this issue can be found in [25].

14.5 Dilepton production

The calculation of dilepton radiation from a medium of strongly interacting partons follows steps very similar to those used for the calculation

of real-photon emission. The first calculation using the HTL resummation technique was performed by Braaten, Pisarski, and Yuan [22]. The dilepton sector has also profited from a reappraisal of the electromagnetic emissivities, complete to leading order in α_s [26]. Instead of concentrating on the techniques that are appropriate for QCD again, we choose to consider radiation from a hot gas of mesons. This is more representative of conditions existing at temperatures below that of the phase transition, or just before the strongly interacting system freezes out. In a similar way, this discussion will illustrate the use of effective interactions to calculate the in-medium vector spectral density, as alluded to in Section 12.2. Conversely, we shall see that the methods in that chapter for inferring the spectral density from experimental data can be used to evaluate the emission of electromagnetic radiation.

This discussion closely follows that of Gale and Kapusta [27]. We start with the interaction between a vector meson and a conserved current. This is known to be renormalizable even if the vector meson is massive. For the case at hand, charged pions interact with a neutral ρ meson via the Lagrangian

$$\mathcal{L} = |D_\mu \Phi|^2 - m_\pi^2 |\Phi|^2 - \tfrac{1}{4}\rho_{\mu\nu}\rho^{\mu\nu} + \tfrac{1}{2}m_\rho^2 \rho_\mu \rho^\mu \qquad (14.78)$$

where Φ is the complex charged pion field, $\rho_{\mu\nu} = \partial_\mu \rho_\nu - \partial_\nu \rho_\mu$ is the ρ field strength, and $D_\mu = \partial_\mu + ig_\rho \rho_\mu$ is the covariant derivative. The one-loop ρ self-energy in a gas of pions is represented by the two diagrams of Figure 14.7. In Euclidean space,

$$\Pi^{\mu\nu}(k) = -g_\rho^2 T \sum_n \int \frac{d^3p}{(2\pi)^3} \frac{(2p+k)^\mu (2p+k)^\nu}{(p^2+m_\pi^2)\left[(p+k)^2+m_\pi^2\right]}$$

$$+ 2\delta^{\mu\nu} g_\rho^2 T \sum_n \int \frac{d^3p}{(2\pi)^3} \frac{1}{p^2+m_\pi^2} \qquad (14.79)$$

Here, p_4 or $k_4 = 2\pi T \times$ an integer. The zero-temperature part of the self-energy may be evaluated using dimensional regularization. The vacuum part is then

$$\Pi_{\text{vac}}^{\mu\nu}(k) = (k^\mu k^\nu - k^2 \delta^{\mu\nu})\frac{1}{3}\left(\frac{g_\rho}{4\pi}\right)^2$$

$$\times \left[\left(1+\frac{4m_\pi^2}{k^2}\right)^{3/2}\ln\left(\frac{\sqrt{1+4m_\pi^2/k^2}+1}{\sqrt{1+4m_\pi^2/k^2}-1}\right) - \frac{8m_\pi^2}{k^2} + C\right]$$

$$(14.80)$$

where C is a renormalization constant. The contribution from $T > 0$ is

$$\Pi^{44}_{\text{mat}}(k) = -\left(\frac{g^2_\rho}{2\pi}\right)\int_0^\infty \frac{dp\,p^2}{\omega}\frac{1}{e^{\beta\omega}-1}\left(\frac{4\omega^2 - k_4^2}{2p|\mathbf{k}|}\ln a - 4 + \frac{2ik_4\omega}{p|\mathbf{k}|}\ln b\right)$$

(14.81)

$$\Pi^{4i}_{\text{mat}}(k) = -\frac{k^i k^4}{\mathbf{k}^2}\Pi^{44}_{\text{mat}}(k)$$

(14.82)

$$\Pi^{ij}_{\text{mat}}(k) = A\delta^{ij} + B\frac{k^i k^j}{\mathbf{k}^2}$$

(14.83)

The scalar functions A and B are given by

$$A = -\frac{1}{2}\left(\frac{g_\rho}{2\pi}\right)^2\int_0^\infty \frac{dp\,p^2}{\omega}\frac{1}{e^{\beta\omega}-1}\left(\frac{4(k_4^2 - \mathbf{k}^2)}{\mathbf{k}^2} - \frac{2ik_4\omega(k_4^2 + \mathbf{k}^2)}{p|\mathbf{k}|^3}\ln b\right.$$
$$\left. + \frac{k_4^2(k_4^2 - 4\omega^2) + \mathbf{k}^2(\mathbf{k}^2 + 2k_4^2 - 4p^2)}{2p|\mathbf{k}|^3}\ln a\right)$$

(14.84)

$$B = -\frac{1}{2}\left(\frac{g_\rho}{2\pi}\right)^2\int_0^\infty \frac{dp\,p^2}{\omega}\frac{1}{e^{\beta\omega}-1}\left(\frac{4(\mathbf{k}^2 - 3k_4^2)}{\mathbf{k}^2} + \frac{2ik_4\omega(3k_4^2 + \mathbf{k}^2)}{p|\mathbf{k}|^3}\ln b\right.$$
$$\left. + \frac{3k_4^2(4\omega^2 - k_4^2) + \mathbf{k}^2(4p^2 - 2k_4^2 - \mathbf{k}^2)}{2p|\mathbf{k}|^3}\ln a\right)$$

(14.85)

with

$$a = \frac{\left(k_4^2 + \mathbf{k}^2 - 2p|\mathbf{k}|\right)^2 + 4\omega^2 k_4^2}{\left(k_4^2 + \mathbf{k}^2 + 2p|\mathbf{k}|\right)^2 + 4\omega^2 k_4^2}$$

$$b = \frac{\left(k_4^2 + \mathbf{k}^2\right)^2 - 4\left(p|\mathbf{k}| + ik_4\omega\right)^2}{\left(k_4^2 + \mathbf{k}^2\right)^2 - 4\left(p|\mathbf{k}| - ik_4\omega\right)^2}$$

(14.86)

and $\omega = \sqrt{p^2 + m_\pi^2}$. Switching back to Minkowski space, we may write as in (5.46)

$$\Pi^{\mu\nu} = FP^{\mu\nu}_{\text{L}} + GP^{\mu\nu}_{\text{T}}$$

(14.87)

where $P^{\mu\nu}_{\text{T/L}}$ are the transverse and longitudinal projection operators. Using the relation between the self-energy and the full and bare

propagators,

$$\Pi^{\mu\nu} = \left(\mathcal{D}^{-1}\right)^{\mu\nu} - \left(\mathcal{D}_0^{-1}\right)^{\mu\nu} \tag{14.88}$$

and (14.87), we obtain

$$\mathcal{D}^{\mu\nu} = -\frac{P_{\mathrm{L}}^{\mu\nu}}{k^2 - m_\rho^2 - F} - \frac{P_{\mathrm{T}}^{\mu\nu}}{k^2 - m_\rho^2 - G} - \frac{k^\mu k^\nu}{m_\rho^2 k^2} \tag{14.89}$$

For any linear response analysis and for lepton pair production rates we need the retarded ρ propagator. Therefore we will analytically continue the Matsubara frequency, $k_4 = 2\pi nT$, to $ik_4 = k_0 = E + i\epsilon$, where $\epsilon \to 0^+$. The scalar functions F and G acquire an imaginary part when a or b are negative. This happens when the variable of integration, p, lies in the interval

$$\left| E\sqrt{1 - 4m_\pi^2/M^2} - |\mathbf{k}| \right| \le 2p \le E\sqrt{1 - 4m_\pi^2/M^2} + |\mathbf{k}| \tag{14.90}$$

Here $M = \sqrt{k^2}$ is the invariant mass of the ρ and $E = \sqrt{M^2 + \mathbf{k}^2}$ is the total energy in the rest frame of the pion gas.

At zero temperature, dimensional regularization and renormalization yield equal longitudinal and transverse self-energies, which are finite:

$$
\begin{aligned}
F_{\mathrm{vac}} &= G_{\mathrm{vac}} \\
&= \frac{g_\rho^2}{48\pi^2} M^2 \left\{ (1 - 4m_\pi^2/M^2)^{3/2} \right. \\
&\quad \times \left. \left(\ln\left| \frac{\sqrt{1 - 4m_\pi^2/M^2} + 1}{\sqrt{1 - 4m_\pi^2/M^2}_1} \right| - i\pi\theta(M^2 - 4m_\pi^2) \right) \frac{8m_\pi^2}{M^2} + C \right\}
\end{aligned}
\tag{14.91}
$$

The bare and renormalized fields and masses are related by

$$\rho_\mu^{(0)} = \mathcal{Z}^{1/2} \rho_\mu \qquad \mathcal{Z}_0 = \left(m_\rho/m_\rho^{(0)} \right)^2 \tag{14.92}$$

and the coupling constants are related by

$$\mathcal{Z}_0 g_\rho^{(0)} = \mathcal{Z}^{1/2} g_\rho \tag{14.93}$$

We may choose $\mathcal{Z}_0 = \mathcal{Z}$ for convenience. Finally, for the physical mass to be m_ρ, we choose C in such a way that $\mathrm{Re}\, F_{\mathrm{vac}}(k^2 = m_\rho^2) = 0$.

Finally, at $T > 0$, $F = F_{\text{vac}} + F_{\text{mat}}$ and $G = G_{\text{vac}} + G_{\text{mat}}$, where

$$F_{\text{mat}} = \frac{g_\rho^2}{4\pi^2} \frac{M^2}{\mathbf{k}^2} \int_0^\infty \frac{dp \, p^2}{\omega} \frac{1}{e^{\beta\omega} - 1}$$

$$\times \left[\frac{4\omega^2 + E^2}{2p|\mathbf{k}|} \left(\ln|a| - i\pi\Delta \right) - 4 + \frac{2\omega E}{p|\mathbf{k}|} \left(\ln|b| + i\pi\Delta \right) \right] \qquad (14.94)$$

$$G_{\text{mat}} = \frac{g_\rho^2}{4\pi^2} \int_0^\infty \frac{dp \, p^2}{\omega} \frac{1}{e^{\beta\omega} - 1} \left[\frac{2(E^2 + \mathbf{k}^2)}{\mathbf{k}^2} - \frac{E\omega M^2}{p|\mathbf{k}|^3} \left(\ln|b| + i\pi\Delta \right) \right.$$

$$\left. + \frac{\mathbf{k}^2(4p^2 - \mathbf{k}^2 + 2E^2) - E^2(E^2 + 4\omega^2)}{4p|\mathbf{k}|^3} \left(\ln|a| - i\pi\Delta \right) \right]$$
$$(14.95)$$

where a and b are given in (14.86) and

$$\Delta = \begin{cases} 1 & \text{if } \left| E\sqrt{1 - 4m_\pi^2/M^2} - |\mathbf{k}| \right| \leq 2p \leq E\sqrt{1 - 4m_\pi^2/M^2} + |\mathbf{k}| \\ 0 & \text{otherwise} \end{cases}$$
$$(14.96)$$

We have shown (14.44) that the dilepton emission rate is related to the imaginary part of the retarded photon self-energy, at finite temperature. The vector meson dominance model (VMD) states that the hadronic electromagnetic current operator is given by the current–field identity

$$J_\mu = -\frac{e}{g_\rho} m_\rho^2 \rho_\mu - \frac{e}{g_\omega} m_\omega^2 \omega_\mu - \frac{e}{g_\phi} m_\phi^2 \phi_\mu \qquad (14.97)$$

The VMD is nonperturbative in the strong interaction and has had an impressive phenomenological success [29]. See also Exercise 14.7. We have encountered VMD before, in Section 12.2. The current–field identity turns the current–current correlation function into a field–field correlation function. Therefore to order e^2 but to all orders in the strong coupling, the dilepton emission rate can be written in terms of the in-medium vector spectral density, which is itself calculated with the effective hadronic Lagrangian:

$$E_+ E_- \frac{d^6 R}{d^3 p_+ d^3 p_-}$$

$$= \frac{2}{(2\pi)^6} \frac{e^4}{g_\rho^2} \frac{m_\rho^4}{M^4} \left(p_+^\mu p_-^\nu + p_+^\nu p_-^\mu - g^{\mu\nu} p_+ \cdot p_- \right) \text{Im} \, \mathcal{D}_{\mu\nu}^{\text{R}}(\omega, \mathbf{k}) \frac{1}{e^{\beta\omega} - 1}$$
$$(14.98)$$

To make the longitudinal and transverse contributions manifest, we may use $k^\mu = p_+^\mu + p_-^\mu$ and $q^\mu = p_+^\mu - p_-^\mu$ to write the expression in terms of
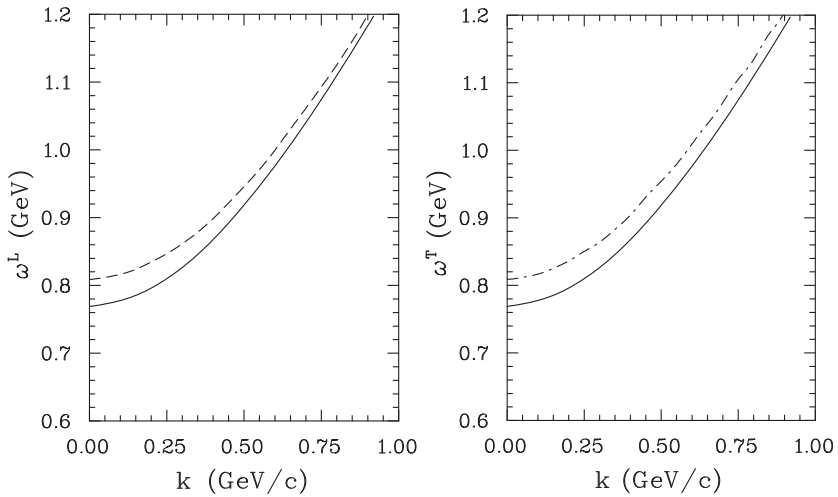
Fig. 14.8.   The dispersion relations for a ρ meson in its longitudinal and transverse polarization states. The curves are for $T = 0$ (lower) and 150 MeV (upper).

the real and imaginary parts of $F = F_{\mathrm{R}} + iF_{\mathrm{I}}$, and $G = G_{\mathrm{R}} + iG_{\mathrm{I}}$:

$$
\begin{aligned}
E_+ E_- & \frac{d^6 R}{d^3 p_+ d^3 p_-} \\
= & \frac{1}{(2\pi)^6} \frac{e^4}{g_\rho^2} \frac{m_\rho^4}{M^4} \left\{ \left[\mathbf{q}^2 - \left(\mathbf{q} \cdot \hat{\mathbf{k}} \right)^2 \right] \frac{-F_{\mathrm{I}}}{\left(M^2 - m_\rho^2 - F_{\mathrm{R}} \right)^2 + F_{\mathrm{I}}^2} \right. \\
& \left. + \left[2M^2 - \mathbf{q}^2 + \left(\mathbf{q} \cdot \hat{\mathbf{k}} \right)^2 \right] \frac{-G_{\mathrm{I}}}{\left(M^2 - m_\rho^2 - G_{\mathrm{R}} \right)^2 + G_{\mathrm{I}}^2} \right\} \frac{1}{e^{\beta\omega} - 1} \quad (14.99)
\end{aligned}
$$

This treatment may be generalized and extended to other mesons [30, 31]. This is necessary for a realistic treatment including chiral symmetry.

Finally, the effects of the interactions on the ρ meson may be quantified further by considering the longitudinal and transverse dispersion relations, which are found by locating the poles in the ρ propagator. They are generated by obtaining the self-consistent solutions of

$$
\begin{aligned}
(\omega^2)^{\mathrm{L}} &= \mathbf{k}^2 + m_\rho^2 + F_{\mathrm{R}}(\omega^{\mathrm{L}}, |\mathbf{k}|, T) \\
(\omega^2)^{\mathrm{T}} &= \mathbf{k}^2 + m_\rho^2 + G_{\mathrm{R}}(\omega^{\mathrm{T}}, |\mathbf{k}|, T)
\end{aligned}
\quad (14.100)
$$

The longitudinal and transverse dispersion relations are plotted in Figure 14.8. Observe that the in-medium energy asymptotically goes over to

the free energy, with increasing momentum. This behavior is characteristic of a many-body effect.

14.6 J/ψ suppression

In the search for the quark–gluon plasma, the experimental signature of this new state of matter that enjoys the most popularity is that associated with the suppression of the J/ψ vector meson. The main ingredients of this simple and elegant idea [32] can briefly be summarized as follows. As the temperature increases, so will the effect of color Debye screening, which will ultimately cause the dissociation of the charmonium bound states. Suppression of the J/ψ was predicted before its experimental observation!

In nonrelativistic charmonium models, the interaction potential is most simply modeled as

$$V(r) = \sigma r - \frac{\alpha_{\text{eff}}}{r} \tag{14.101}$$

where σ is the string tension and α_{eff} is an effective Coulombic interaction coupling. The energy of the lowest bound state can be roughly estimated in a semiclassical approximation [32]. We start by writing

$$E(r) = 2m + \frac{1}{mr^2} + V(r) \tag{14.102}$$

where m is the c quark rest mass. The second term is obtained by invoking the uncertainty relation to write the kinetic term involving the reduced mass in coordinate space. The lowest bound state is found by minimizing the energy with respect to r. Taking $\alpha_{\text{eff}} \simeq 1/2$, $m \simeq 1.5$ GeV, and $\sigma = 0.19$ GeV^2 one obtains $r_{J/\psi} \simeq 0.3$ fm. This value is in qualitative agreement with that obtained through more sophisticated approaches and also confirms that, at $T = 0$, the size of the J/ψ is largely set by the confining part of the potential.

Now consider the high-temperature plasma phase. If the transition is first order, this is tantamount to choosing $T > T_c$. Since the quark–antiquark pair is heavy, it makes sense to use a static potential for their mutual interaction. We have discussed this already in Chapters 8 and 10. At leading order in the coupling, the interaction is modeled by one-gluon exchange, and at small momenta the gluon propagator develops an electric mass related to $\Pi_{00}(k)$. In pure SU(N) gauge theory, one calculates the real part of the finite-temperature one-loop gluon self-energy.

The Debye-screened color Coulomb potential is

$$V(r) = -\frac{N^2 - 1}{2N} \frac{g^2}{4\pi r} \exp(-m_{\text{el}}r) = -\frac{\alpha_{\text{s}}^{\text{eff}}}{r} \exp(-m_{\text{el}}r) \tag{14.103}$$

with $m_{\mathrm{el}}^2 = Ng^2T^2/3$. The coupling $\alpha_{\mathrm{s}}^{\mathrm{eff}}$ obtained above T_{c} is generally different from that used in the zero-temperature potential (14.101). Using [33]

$$g^2(T) = \frac{24\pi^2}{11N \ln\left(19.2T/\Lambda_{\overline{\mathrm{MS}}}\right)} \tag{14.104}$$

one may get an estimate for $T \sim \Lambda_{\overline{\mathrm{MS}}}$, which implies that $\alpha_{\mathrm{s}}^{\mathrm{eff}} \simeq 0.3$.

An interesting phenomenon, revealed by keeping the first powers in the momentum expansion of Π_{00}, is that of Friedel oscillations in QCD [33]. To see this, it is useful to recall that $F = -\Pi_{00} = F_{\mathrm{vac}} + F_{\mathrm{mat}}$. A low-momentum expansion for $F_{\mathrm{mat}}(0, \mathbf{k})$ has been performed in the temporal axial gauge and is [34]

$$
\begin{aligned}
F_{\mathrm{mat}}(0, \mathbf{k}) = \ & \frac{1}{3}g^2NT^2 - \frac{1}{4}g^2NT|\mathbf{k}| \\
& - \frac{11}{48\pi^2}g^2N\mathbf{k}^2 \left[\ln\left(\frac{\mathbf{k}^2}{T^2}\right) + \frac{2}{33} + 2(\gamma_{\mathrm{E}} - \ln 4\pi) \right]
\end{aligned}
\tag{14.105}
$$

The first term in this expansion is the electric mass, which is gauge invariant. The second term, linear in $\mathbf{k}$, is also gauge invariant. It is the same in the temporal-axial, Coulomb, and all covariant gauges. The reason is that this term modifies the plasmon effect in the thermodynamic potential; see Section 8.3. The next term has the same coefficient as that of the vacuum term, as it must in order to produce a temperature-dependent coupling constant. Keeping the terms that are subleading in the low-momentum expansion produces

$$V(r) = -\frac{N^2 - 1}{2N} \frac{g^2(T)}{2\pi^2 r} \int_0^\infty dz \, \frac{z \sin zx}{z^2 - 2tz + 1} \tag{14.106}$$

where $x = m_{\mathrm{el}}r$ and $t = 3m_{\mathrm{el}}/8T$. A contour integration puts the integral into the form

$$V(r) = -\frac{N^2 - 1}{2N} \frac{g^2(T)}{4\pi r} S(x, t) \tag{14.107}$$

The dimensionless screening function is

$$
\begin{aligned}
S(x, t) = \ & 2 \left(\cos tx + \frac{t}{\sqrt{1 - t^2}} \sin tx \right) \exp\left(-x^2\sqrt{1 - t^2} \right) \\
& - \frac{4t}{\pi} \int_0^\infty dy \, \frac{y^2 \exp(-xy)}{(1 - y^2)^2 + 4t^2 y^2}
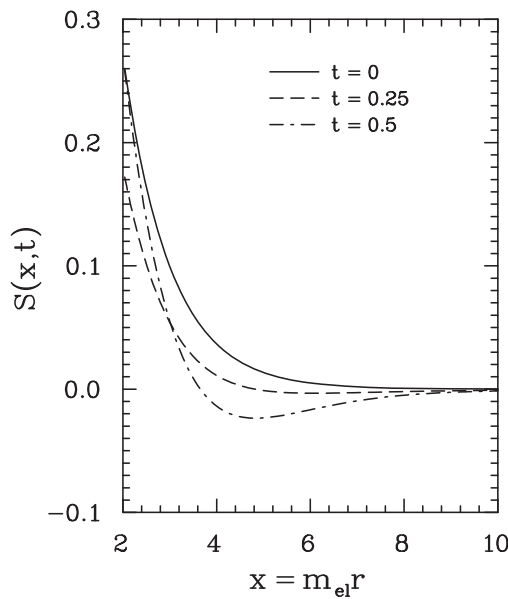\end{aligned}
\tag{14.108}
$$

Fig. 14.9.   The screening function $S(x, t)$ for different values of $t = 3m_{\text{el}}/8T$.

$S(x, t)$ has the following asymptotic expansion. For fixed x and small t (the high-temperature limit), $S \to e^{-x}$, the Debye-screening result. For fixed t and $x \to \infty$ (the long-distance limit), $S \to 8t/\pi x^3$. At very large distances the potential is repulsive and falls as a power, not as an exponential:

$$V(r) \to \frac{9}{4\pi^3} \left[\frac{N^2 - 1}{N^2} \right] \frac{1}{T^3 r^4}$$

The screening function is derived under the assumption that $x > 1$; that is, the low-momentum expansion of $F(0, \mathbf{k})$ has been used. This expression cannot be written in terms of elementary functions. The integration in (14.108) must be done numerically, and the results are plotted in Figure 14.9. We see that in general the inclusion of the momentum dependence of the gluon self-energy increases the screening for $1 < x < 3$ (or between one and three Debye lengths) but decreases the screening at greater distances. In fact, for large distances there is a slight antiscreening: the potential is repulsive instead of attractive.

Going back to the low-momentum expansion, we keep only the leading term. Inserting (14.103) into (14.102) and minimizing produces a value for $r_{J/\psi}$. All the temperature dependence is now contained in the

value of m_{el}. After minimization, the algebraic equation to be solved is

$$\frac{2m_{\text{el}}}{m\alpha_{\text{eff}}} = x(x+1)\mathrm{e}^{-x} \tag{14.109}$$

where $x = rm_{\text{el}}$. Notice that the left-hand side increases linearly with temperature (the variation of α_{eff} with T is only logarithmic). The right-hand side has a maximum at 1.62. At that point we have $(m_{\text{el}})_{\max} = 0.81m\alpha_{\text{s}}^{\text{eff}}$. Extracting the logarithmic dependence, and using the definition of the electric mass, yields the equation

$$T = \frac{0.81}{3\pi}\, mg(T) \tag{14.110}$$

Using $\Lambda_{\overline{\text{MS}}} = 220$ MeV, the above turns into a nonlinear equation for the maximum temperature at which the J/ψ exists. Solving it, one obtains $T_{\max} \simeq 200$ MeV. Should the J/ψ disappear because of the mechanism discussed here, the higher-lying excitations of the charmonium bound states will already have dissolved. Remember that the J/ψ is an $n = 1$, $\ell = 0$ state, whereas the lesser-bound states are $\psi'(n = 2,\, \ell = 0)$ and $\chi_{\text{c}}(n = 2,\, \ell = 1)$.

The whole analysis in terms of potential models can only give a general idea of the dissociation pheomenon. First, the heavy quark potential should be determined directly using lattice QCD simulations at finite temperature. The nonperturbative studies could allow the study of the evolution of the gap between the charmonium bound-state mass and the open charm threshold, among other things. It has recently become possible to study directly the finite-temperature charmonium spectral density on the lattice [35]. All such studies are currently based on quenched lattices: they do not include quark loops, thermal or otherwise. This obvious shortcoming will have to be addressed in order to extract any quantitative result. Furthermore, one needs to reconstruct the thermal spectral densities from the thermal correlators: recent progress on this has been made possible by the use of Bayesian techniques in lattice analysis [36]. This topic is one for specialists. See Chapter 10 for the basic notions of QCD lattice gauge theory.

Any analysis of the charmonium spectrum in nuclear collisions will be incomplete unless supplemented by knowledge of what happens to those states in cold nuclear matter and in hot hadronic systems. These are all environments that are liable of influencing the measured J/ψ yields as well as those of the higher-lying states. There is at present considerable uncertainty, because the J/ψ sits at an energy scale that is not high enough for perturbative QCD to be totally reliable and because there is no direct experimental data on J/ψ–hadron cross sections. However, the yields of charmonium bound states as a function of the muon pair
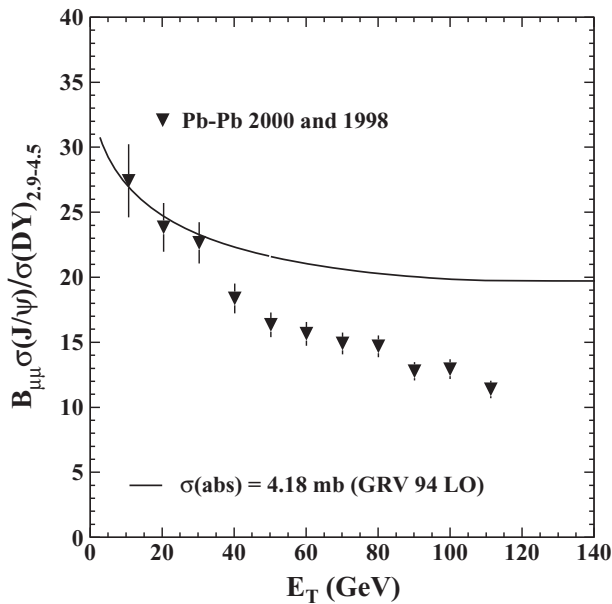
Fig. 14.10. The average of two data sets showing the J/ψ to Drell–Yan ratio (multiplied by the branching ratio into a dimuon pair) as a function of the transverse energy, in the invariant mass region 2.9 GeV/c^2 < M < 4.5 GeV/c^2. The solid line shows the effect of nuclear absorption with an absorption cross section that is extracted from proton–nucleus data. This plot is from [37], with kind permission of Springer Science and Business Media.

transverse energy (and hence of event-centrality) in proton–nucleus collisions can reveal the features that are germane to absorption in cold nuclear matter. In fact, proton–nucleus analyses provide an important class of control experiments, as plasma formation is not expected to occur there. Drell–Yan muon pairs serve as a background estimator, as they constitute the dominant source of continuum dileptons at the invariant masses of interest here. The ratios of cross sections for proton–nucleus collisions are then fitted to a Glauber prescription of normal nuclear matter absorption; this procedure leads to a value $\sigma_{\mathrm{abs}} = 4.18 \pm 0.35$ mb [37]. The extra absorption in nucleus–nucleus events, shown in Figure 14.10, is then deemed anomalous. Owing to the large multiplicities that are common in heavy ion collision environments, the interaction of the newly formed J/ψ with this hot hadronic matter also has to be considered. At the present time, many hadronic approaches claim to reproduce the anomalous SPS J/ψ absorption data with various degrees of success, thereby making the arguments claiming a a new state of matter considerably less compelling. This topic is still under investigation and will continue to be so in experimental measurements at RHIC and at the LHC.
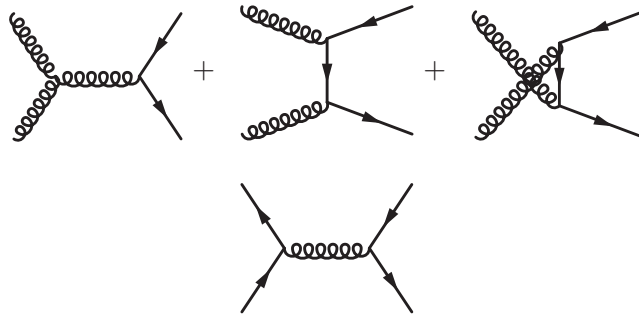
Fig. 14.11.   Tree-level diagrams for the processes $gg \to s\bar{s}$, and $q\bar{q} \to s\bar{s}$.

14.7 Strangeness production

Another signature of the presence of a nascent quark–gluon plasma created in high-energy nuclear collisions is that of strangeness production [38]. Strange quarks and antiquarks are absent in cold nuclear matter. They are found only in the parton distribution functions of the sea quarks, probed by deep inelastic scattering experiments. As a consequence their abundances are typical of those of quantum fluctuations. In a hot partonic system, however, the situation is different. High initial temperatures, greater than the strange quark mass, imply an abundance comparable with that of the lighter up and down quarks. The loss of confinement suggests comparable rates of production of up, down, and strange quarks.

Starting with no strange quarks (or antiquarks), estimates for the production of $s\bar{s}$ pairs can be obtained from lowest-order perturbative QCD. The contributing channels are those of gluon fusion and light $q\bar{q}$ annihilation. The relevant Feynman diagrams are shown in Figure 14.11. The invariant matrix elements have been calculated by several groups of workers to leading order in the strong coupling constant [39]. Labeling the processes in Figure 14.11 by a, b, c and d, respectively (going from left to right, starting from the top), the squared matrix elements summed over initial color, spin, and flavor states are

$$
\begin{aligned}
\sum |\mathcal{M}_a|^2 &= 16 \times 6(\pi\alpha_{\mathrm{s}})^2 \frac{(m^2 - t)(m^2 - u)}{3s^2} \\
\sum |\mathcal{M}_b|^2 &= 16 \times 6(\pi\alpha_{\mathrm{s}})^2 \frac{2}{27} \frac{(m^2 - t)(m^2 - u) - 2m^2(m^2 + t)}{(m^2 - t)^2} \\
\sum |\mathcal{M}_\mathrm{c}|^2 &= 16 \times 6(\pi\alpha_{\mathrm{s}})^2 \frac{2}{27} \frac{(m^2 - t)(m^2 - u) - 2m^2(m^2 + u)}{(m^2 - u^2)^2} \\
\sum |\mathcal{M}_d|^2 &= N_{\mathrm{f}}\, 6^2(\pi\alpha_{\mathrm{s}})^2 \frac{16}{81} \frac{(m^2 - t)^2 + (m^2 - u)^2 + 2m^2 s}{s^2}
\end{aligned}
\tag{14.111}
$$

the interference terms being

$$\sum \mathcal{M}_a \mathcal{M}_b^* = 16 \times 6 \, (\pi\alpha_{\mathrm{s}})^2 \frac{(m^2 - t)(m^2 - u) + m^2(u - t)}{12s(m^2 - t)}$$

$$\sum \mathcal{M}_a \mathcal{M}_c^* = 16 \times 6 \, (\pi\alpha_{\mathrm{s}})^2 \frac{(m^2 - t)(m^2 - u) + m^2(u - t)}{12s(m^2 - u)} \quad (14.112)$$

$$\sum \mathcal{M}_b \mathcal{M}_c^* = 16 \times 6 \, (\pi\alpha_{\mathrm{s}})^2 \frac{m^2(s - 4m^2)}{108(m^2 - u)(m^2 - t)}$$

Here s, t, and u are the usual Mandelstam variables, N_{f} is the number of fermion flavors, and m is the strange quark mass. In the equations above, the numerical prefactors correspond to products of the degeneracy factors (spin × color) for the gluons (2×8) and quarks (2×3). For the processes under consideration a scale appropriate for the evaluation of the strong coupling yields $\alpha_{\mathrm{s}}(s)$.

Given the above, the cross sections averaged over initial states are evaluated to be

$$\bar{\sigma}_{gg \to s\bar{s}} = \frac{2\pi\alpha_{\mathrm{s}}^2}{3s} \left[\left(1 + \frac{4m^2}{s} + \frac{m^4}{s^2}\right) \tanh^{-1} w(s) - \left(\frac{7}{8} + \frac{31}{8}\frac{m^2}{s}\right) w(s) \right]$$

$$\bar{\sigma}_{q\bar{q} \to s\bar{s}} = \frac{8\pi\alpha_{\mathrm{s}}^2}{27s} \left(1 + \frac{2m^2}{s}\right) w(s) \quad (14.113)$$

where $w(s) = \sqrt{1 - 4m^2/s}$. The rate for pair production can then be calculated using the usual formalism of relativistic kinetic theory. Quite generally, one may write a rate for the reaction $a_1 + a_2 \to X$, in the independent-particle limit, as

$$R(a_1 + a_2 \to X) = \frac{1}{1 + \delta_{a_1, a_2}} \int \frac{d^3 k_1}{(2\pi)^3} f(\mathbf{k}_1) \frac{d^3 k_2}{(2\pi)^3} f(\mathbf{k}_2) \sigma(a_1 + a_2 \to X) \, v_{\mathrm{rel}}$$

$$(14.114)$$

with

$$v_{\mathrm{rel}} = \frac{(k_1 \cdot k_2)^2 - m_a^4}{E_1 E_2} \quad (14.115)$$

In the case where the initial-state fields are massless, $v_{\mathrm{rel}} = s/(2E_1 E_2)$ with $s = (k_1 + k_2)^2$.

The invariant rate (the number of reactions per unit time per unit volume) is then

$$R = \frac{d^4 N}{dt \, d^3 x} = \frac{1}{2} \int_{4m^2}^{\infty} ds \, s \, \delta(s - (k_1 + k_2)^2) \int \frac{d^3 k_1}{(2\pi)^3 E_1} \int \frac{d^3 k_2}{(2\pi)^3 E_2}$$

$$\times \left(\frac{1}{2} f_g(\mathbf{k}_1) f_g(\mathbf{k}_2) \bar{\sigma}_{gg \to s\bar{s}}(s) + N_{\mathrm{f}} \, f_q(\mathbf{k}_1) f_{\bar{q}}(\mathbf{k}_2) \bar{\sigma}_{q\bar{q} \to s\bar{s}}(s) \right)$$

$$(14.116)$$

Note that the distribution functions here contain the appropriate degeneracy factor,

$$f_g(\mathbf{k}) = 16 \frac{1}{e^{\beta|\mathbf{k}|} - 1}$$

so that the gluon density is

$$n_g = \frac{N_g}{V} = \int \frac{d^3k}{(2\pi)^3} f_g$$

and similarly for the quarks and antiquarks.

Inserting the appropriate Bose–Einstein or Fermi–Dirac distribution functions, the net rate may be computed numerically. Doing this with the quark chemical potential set to zero, one finds that the gluon contribution dominates the contribution with the $q\bar{q}$ initial state. For the gluon fusion rate, expanding the Bose–Einstein distribution functions for $T \ll m$ yields

$$\begin{aligned}
R_g &= \frac{4T}{\pi^4} \int_{4m^2}^{\infty} ds\, s^{3/2} \bar{\sigma}_{gg \to s\bar{s}} \sum_{k,\ell=1}^{\infty} \frac{1}{\sqrt{k\ell}} K_1\left(\frac{\sqrt{k\ell s}}{T}\right) \\
&\simeq \frac{7}{6\pi^2} \alpha_s^2 m T^3 e^{-2m/T} \left(1 + \frac{51}{14}\frac{T}{m} + \cdots\right)
\end{aligned} \tag{14.117}$$

One may divide out the temperature dependence and plot a dimensionless rate, $R/\alpha_s T^4$, against m/T, where m is the strange quark mass. A parametrization of these results over the temperature range considered here is perhaps useful for modeling purposes. An excellent parametrization for the range of m/T plotted is provided by $R/\alpha_s^2 T^4 = (a + bx^2)\exp(-cx)$, with $x = m/T$, $a = 0.937$, $b = 0.958$, and $c = 2.715$. The fit is shown, together with the result of the numerical rate calculation, in Figure 14.12.

When the density of $s\bar{s}$ pairs increases, their annihilation will start to deplete the population of strange quarks. This depletion rate will be proportional to the square of the strange quark density. Then the rate equation for a static (nonexpanding) system is

$$\frac{dn_s(t)}{dt} = R \left[1 - \left(\frac{n_s(t)}{n_s^{eq}}\right)^2\right] \tag{14.118}$$

For small departures from equilibrium, such that $n(t) = n^{eq} + \delta n(t)$ where $|\delta n(t)| \ll n^{eq}$, we may linearize (14.118):

$$\frac{d\,\delta n_s(t)}{dt} = -\frac{\delta n_s(t)}{\tau_{eq}} \qquad \tau_{eq} = \frac{n_s^{eq}}{2R} \tag{14.119}$$

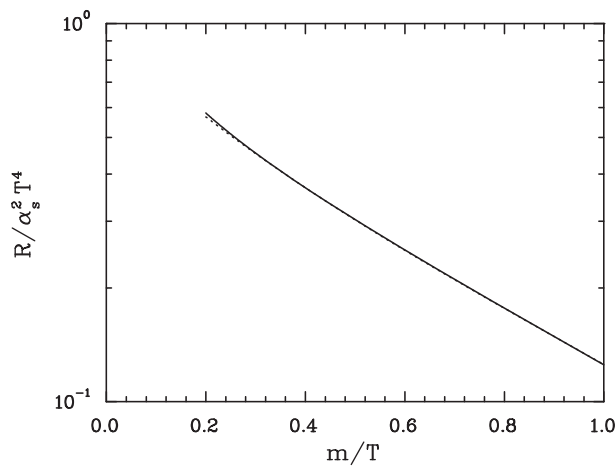Therefore, a large rate means a short equilibration time.

Fig. 14.12.   The dimensionless rate for emission of $s\bar{s}$ pairs from a sum of all tree-level partonic processes with u and d quarks, as a function of the ratio of the strange quark mass to the temperature (solid line). Here $\alpha_{\rm s} = 0.6$ and $m = 150$ MeV. The parametrization discussed in the text corresponds to the dotted line.

We now consider the fate of the strange hadrons in the portion of the system's spacetime trajectory that is in the confined sector. Let us assume that the system has zero net baryon number and that the species present are light pseudoscalars only. Anticipating the effect of high temperatures, we approximate the distribution functions to be of the Boltzmann type with vanishing chemical potentials. Then all integrals but one can be performed in (14.114), to yield

$$R(a_1 + a_2 \to X) = \frac{T^6}{16\pi^4} \int_{z_0}^\infty \sigma(E) z^2 (z^2 - 4z_a^2) K_1(z)\, dz \quad (14.120)$$

where $z = E/T$, E is the center-of-mass energy, and $z_a = m_a/T$. For the annihilation process, $z_0 = 2z_a$. If $a_1 + a_2 \to b + c$ and $2m_a < m_b + m_c$ then $z_0 = (m_b + m_c)/T$. The reader is invited to verify that this expression agrees with the leading term ($k = \ell = 1$) in (14.117).

There is not much data on strangeness production in mesonic annihilation. Some estimates exist of the cross section for the process $\pi^+\pi^- \to K^+K^-$ from measurements of $\pi^- p \to K^+K^- n$ [40]. These estimates find that the cross section is roughly constant as a function of energy, with a mean value of $\sigma_0 = 5/3$ mb. With a total of three isospin channels, the total cross section is thus $3\sigma_0 = 5$ mb. Then

$$R(\pi\pi \to K\bar{K})$$
$$= \frac{3\sigma_0 T^6}{16\pi^4} \left[z_0^2(z_0^2 - 4z_a^2 + 8)K_0(z_0) + 4z_0(z_0^2 - 2z_a^2 + 4)K_1(z_0) \right] \quad (14.121)$$
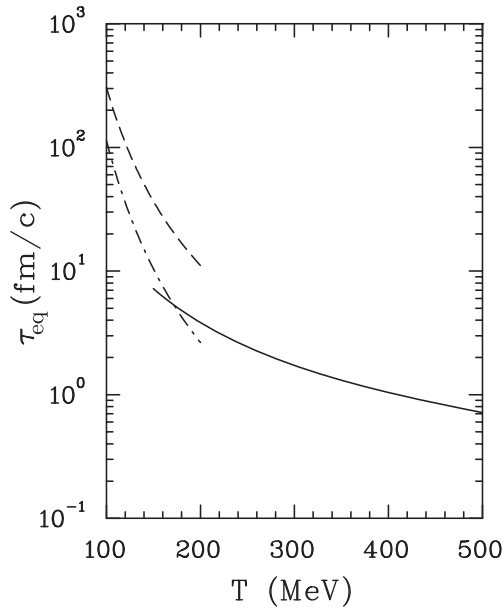
In this case, $z_0 = 2m_K/T$ and $z_a = m_\pi/T$.

Fig. 14.13.   The time constant τ_{eq} for chemical equilibration as a function of temperature for different processes: solid curve, τ_{eq} for the partonic reactions $gg \to s\bar{s}$ and $q\bar{q} \to s\bar{s}$ (with $q = u$, d); broken curve, τ_{eq} for $\pi\pi \to K\bar{K}$; broken and dotted curve, the equilibration time for the $K\bar{K}$ annihilation processes. The parameters used here are $\alpha_{\text{s}} = 0.6$ and m (strange quark mass) = 150 MeV.

Another useful reaction for evaluating the population of strangeness-carrying hadrons is $K^+ K^- \to$ nonstrange hadrons. Its magnitude may be estimated from that of $p\bar{p} \to$ charged hadrons [41]:

$$\sigma(p\bar{p} \to \text{charged hadrons}) = A' + \frac{B'}{\sqrt{(E/m_p)^2 - 4}} \qquad (14.122)$$

with $A' = 38.25$ mb and $B' = 36$ mb. Since $K^+ K^-$ has four valence quarks whereas $p\bar{p}$ has six, a simple estimate may then be obtained by multiplying A' and B' by $(2/3)^2$ and replacing m_p by m_K. Finally, bear in mind that a K^- can equally annihilate on a K^0 or a K^+. Putting all this together we arrive at

$$R(K\bar{K} \text{ annihilation}) = 2(R_A + R_B)$$

where

$$R_A = \frac{AT^6}{8\pi^4} z_0^3 K_3(z_0)$$

$$R_B = \frac{BT^6}{64\pi^3} z_0 (3 + 3z_0 + z_0^2) \mathrm{e}^{-z_0}$$

(14.123)

with $z_0 = 2m_K/T$, $A = 17$ mb, and $B = 16$ mb. It is revealing to plot the relevant strangeness-equilibration time constants, as evaluated from (14.119). The rates were integrated numerically in the Boltzmann limit for the distribution functions and were used to obtain the various relaxation times. These are shown in Figure 14.13. Of course, not all processes operate over the complete temperature range shown there.

This figure is revealing in many aspects. First, note the strong temperature-dependence. Second, this plot shows why strangeness-enhancement is considered a promising probe for the formation of the quark–gluon plasma. The smallness of τ_{eq} for the partonic contributions indicates that gluons and light quarks will reach equilibrium during the early stages of the plasma phase. However, note that the time constant for $s\bar{s}$ in the plasma phase is within a factor 2 of that for $K\bar{K}$ annihilation in the hadron phase for the interesting temperature interval of $150 < T < 250$ MeV. This suggests that strangeness production and annihilation in the hadronic phase will be comparable in magnitude with that in the plasma phase. This also means that the actual usefulness of this observable will depend on the details of the evolution scenario. Finally, the relationship between the rates for $\pi\pi \to K\bar{K}$ and for $K\bar{K}$ annihilation is as it should be. If the latter pairs could only annihilate into a pair of pions, the two rates would be equal by detailed balance. However, two kaons may annihilate into a many-pion (more than two) final state, and this will increase the net rate and decrease the related time constant.

In order to calculate how the strangeness density evolves in time, the spacetime evolution is needed. An increase in volume will cause a proportionate decrease in density even in the absence of interactions. This means that (14.118) needs to be supplemented by a dilution term:

$$\frac{dn_{\mathrm{s}}(t)}{dt} = R \left[1 - \left(\frac{n_{\mathrm{s}}(t)}{n_{\mathrm{s}}^{\mathrm{eq}}} \right)^2 \right] - \frac{n_{\mathrm{s}}(t)}{V(t)} \frac{dV(t)}{dt}$$

(14.124)

In the Bjorken model, the volume grows linearly with time because the entropy density drops inversely with time, (14.10). Therefore in this case

$$\frac{dn_{\mathrm{s}}(t)}{dt} = R(T(t)) \left[1 - \left(\frac{n_{\mathrm{s}}(t)}{n_{\mathrm{s}}^{\mathrm{eq}}} \right)^2 \right] - \frac{n_{\mathrm{s}}(t)}{t}$$

(14.125)

The initial condition, $n_s(t_0)$, needs to be chosen. Three possibilities include: (i) no strange quarks; (ii) strange quarks in chemical equilibrium; (iii) a strange quark abundance determined by proton–proton collisions at the same energy. If the equilibration rate is high enough compared with the expansion rate, strange quarks will come to equilibrium no matter what the initial condition.

The equation above is valid in the plasma phase. Once the plasma begins to convert into hadrons, the rate equation for kaons is

$$\frac{dn_{K^-}(t)}{dt} = R_h(T_c) \left(1 - \left(\frac{n_{K^-}(t)}{n_{K^-}^{eq}(T_c)} \right)^2 \right)$$
$$- \frac{n_{K^-}(t)}{\hat{f}(t)\,t} \frac{d}{dt} \left[\hat{f}(t)\,t \right] + \frac{1}{2} \frac{n_s(t)}{\hat{f}(t)} \frac{d\hat{f}(t)}{dt} \qquad (14.126)$$

where $\hat{f}(t) = 1 - f(t)$ is the volume fraction in the plasma phase and R_h is the rate in the hadron phase. The dilution term is slightly different from its previous version. The last term given the gain from strangeness conversion into the hadron phase from the plasma phase. The factor $1/2$ accounts for the fact that a given s quark is equally likely to end up in a $\bar{K}^0$.

The strangeness content as a function of time is given by integration of the differential equations presented in this section. It is clear how to adapt this rate equation to the evolution in the purely hadronic phase. When comparing with actual measurements, perhaps a more realistic estimate will need to include multistrange baryons and strange antibaryons, as well as to consider the effect of different and more sophisticated spacetime evolution scenarios. The interested reader is invited to consult the research literature for the current status of strangeness as a probe of heavy ion collisions.

14.8 Exercises

14.1   Construct the pressure and energy density as functions of temperature for the three equations of state presented in Section 14.1.

14.2   A simple way to model the effect of the transition from one-dimensional to three-dimensional expansion is to replace the formula $s(\tau) = s(\tau_0)\tau_0/\tau$ in the Bjorken model by $s(\tau) = [s(\tau_0)\tau_0 R^2]/[\tau(\tau^2 + R^2)]$, where R is the nuclear radius. This takes into account the time delay for the rarefaction wave from the surface to reach the center of the hot matter. Calculate the temperature as a function of proper time for the three equations of state of Section 14.1, and plot the result similarly to Figure 14.2.

14.3 Derive the expression for the photon production rate in relativistic kinetic theory (14.46).

14.4 Consider the rates for photon emission through the Compton and annihilation processes, (14.54) and (14.55). These were evaluated assuming that the initial-state distribution functions could be approximated by their Maxwell–Boltzmann form. Show that, keeping the quantum distribution functions in the initial state, the rates from the Compton and annihilation processes become [42]

$$E\frac{d^3R}{d^3p}^{\text{Compton}} = \frac{5}{9}\frac{\alpha\alpha_{\text{s}}}{4\pi^2}\frac{1}{e^{E/T}+1}T^2\left[\ln\left(\frac{4ET}{k_{\text{c}}^2}\right) + C_{\text{F}}'\right]$$

where

$$C_{\text{F}}' = -\gamma_{\text{E}} + \frac{1}{2} - \frac{8}{\pi^2}\sum_{n=0}^{\infty}\ln\frac{(2n+1)}{(2n+1)^2}$$

and

$$E\frac{d^3R}{d^3p}^{\text{annihilation}} = \frac{5}{9}\frac{\alpha\alpha_{\text{s}}}{4\pi^2}\frac{1}{e^{E/T}+1}T^2\left[\ln\left(\frac{4ET}{k_{\text{c}}^2}\right) + C_{\text{B}}'\right]$$

where

$$C_{\text{B}}' = -\gamma_{\text{E}} - 1 - \frac{8}{\pi^2}\sum_{n=0}^{\infty}\ln\frac{(2n+1)}{(2n+1)^2}$$

14.5 Prove (14.65).

14.6 Derive the expressions (14.94) and (14.95) for the scalar functions F and G at finite temperature.

14.7 Show that the pion electromagnetic form factor in the vector meson dominance model (VMD) is predicted to be

$$F_\pi(M) = \frac{m_\rho^2 + F_{\text{vac}}(0)}{m_\rho^2 + F_{\text{vac}}(M) - M^2}$$

and show that this reproduces the Gounaris–Sakurai formula [28].

14.8 Construct the grand canonical partition function for a gas of hadrons containing all light mesons, baryons, and resonances, up to a mass of 2 GeV. Use the *Particle Data Table* [43]. For several combinations of temperature and chemical potential (say $T = 100$, 150, and 200 MeV; $\mu_B = 250$ and 550 MeV), evaluate the density of positively charged pions (including the resonance-decay contribution) divided by that of the thermal pions.

14.9   Calculate numerically the rate in (14.116), and show that the contribution from quark–antiquark annihilation is negligible with respect to the gluon fusion rate. You should plot the two rates for $100 < T < 300$ MeV.

14.10   Assuming a first-order phase transition, obtain the behavior of the strangeness density as a function of time in the Bjorken model. Do the calculation for two initial temperatures, $T_0 = 250$ and 500 MeV. Plot $n_s(t)/n_s^{\text{eq}}$ as a function of time, and compare with the results shown in [44].

References

1. Fermi, E., *Phys. Rev.* **81**, 83 (1951).
2. Landau, L. D., *Izv. Akad. Nauk SSSR, ser. fiz.* **17**, 51 (1953).
3. Bjorken, J. D., *Phys. Rev. D* **27**, 140 (1983).
4. Chodos, A., Jaffe, R. L., Johnson, K., Thorn, C. B., and Weisskopf, V. F., *Phys. Rev. D* **9**, 3471 (1974).
5. Becattini, F., *Z. Phys. C* **69**, 485 (1996).
6. Braun-Munzinger, P., Redlich, K., and Stachel, J. (2003). In *Quark–Gluon Plasma 3* (World Scientific, Singapore).
7. Cleymans, J., and Redlich, K., *Phys. Rev. Lett.* **81**, 5284 (1998); *Phys. Rev. C* **60**, 054908 (1999).
8. Cleymans, J., Oeschler, H., and Redlich, K., *Phys. Rev. C* **59**, 1663 (1999); Averbeck, R., Holzmann, R., Metag, V., and Simon, R. S., *Phys. Rev. C* **67**, 024903 (2003); Becattini, F., Cleymans, J., Keranen, A., Suhonen, E., and Redlich, K., *Phys. Rev. C* **64**, 024901 (2001).
9. Braun-Munzinger, P., Stachel, J., Wessels, J. P., and Xu, N., *Phys. Lett.* **B344**, 43 (1995); **B365**, 1 (1996); Braun-Munzinger, P., Heppe, I., and Stachel, J., *Phys. Lett.* **B465**, 15 (1999); Becattini, F., Gazdzicki, M., Keranen, A., Manninen, J., and Stock, R., *Phys. Rev. C* **69**, 024905 (2004).
10. Redlich, K., and Tounsi, A., *Eur. Phys. J. C* **24**, 589 (2002).
11. Braun-Munzinger, P., Magestro, D., Redlich, K., and Stachel, J., *Phys. Lett.* **B518**, 41 (2001); Cleymans, J., Kampfer, B., Kaneta, M., Wheaton, S., and Xu, N., *Phys. Rev. C* **71**, 054901 (2005); Broniowski, W., and Florkowski, W., *Phys. Rev. C* **65**, 064905 (2002).
12. Letessier, J., and Rafelski, J. (2002). *Hadrons and Quark–Gluon Plasma* (Cambridge University Press, Cambridge).
13. Gerber, P., Leutwyler, H., and Goity, J. L., *Phys. Lett.* **B246**, 513 (1990).
14. Bleicher, M., and Aichelin, J., *Phys. Lett.* **B530**, 81 (2002): Bravina, L., *et al.*, *Nucl. Phys.* **A698**, 383 (2002); *Phys. Rev. C* **66**, 014906 (2002).
15. Shuryak, E. V., *Sov. J. Nucl. Phys.* **28**, 408 (1978).
16. Kajantie, K., and Miettinen, H. I., *Z. Physik* **C9**, 341 (1981).
17. Halzen, F., and Liu, H. C., *Phys. Rev. D* **25**, 1842 (1982).
18. Sinha, B., *Phys. Lett.* **B128**, 91 (1983).
19. Hwa, R. C., and Kajantie, K., *Phys. Rev. D* **32**, 1109 (1985).

20. Staadt, G., Greiner, W., and Rafelski, J., *Phys. Rev. D* **33**, 66 (1986).
21. Kapusta, J., Lichard, P., and Seibert, D., *Phys. Rev. D* **44**, 2774 (1991).
22. Braaten, E., Pisarski, R. D., and Yuan, T. C., *Phys. Rev. Lett.* **64**, 2242 (1990).
23. Aurenche, P., Gélis, F., Kobes, R., and Petitgirard, E., *Phys. Rev. D* **54**, 5274 (1996); Aurenche, P., Gélis, F., Kobes, R., and Zaraket, H., *Phys. Rev. D* **58**, 085003 (1998).
24. Arnold, P., Moore, G. D., and Yaffe, L. G., *JHEP*, **0112**, 9 (2001); **0206**, 30 (2002).
25. Turbide, S., Rapp, R., and Gale, C., *Phys. Rev. C* **69**, 014903 (2004).
26. Aurenche, P., Gélis, F., Moore, G. D., and Zaraket, H., *JHEP* **0212**, 6 (2002).
27. Gale, C., and Kapusta, J. I., *Nucl. Phys.* **B357**, 65 (1991).
28. Gounaris, G. J. and Sakurai, J. J., *Phys. Rev. Lett.* **21**, 244 (1968).
29. Sakurai, J. J. (1969). *Currents and Mesons* (University of Chicago Press, Chicago).
30. Rapp, R., and Wambach, J., *Adv. Nucl. Phys.* **25**, 1 (2000).
31. Rapp, R., and Gale, C., *Phys. Rev. C* **60**, 024903 (1999).
32. Matsui, T., and Satz, H., *Phys. Lett.* **B178**, 416 (1986).
33. Gale, C., and Kapusta, J., *Phys. Lett.* **B198**, 89 (1987).
34. Kajantie, K., and Kapusta, J., *Ann. Phys. (NY)* **160**, 477 (1985).
35. Datta, S., Karsch, F., Petreczky, P., and Wetzorke, I., *Phys. Rev. D* **69**, 094507 (2004).
36. Asakawa, M., Hatsuda, T., and Nakahara, Y., *Prog. Part. Nucl. Phys.* **46**, 459 (2001).
37. Alessandro, B., *et al.*, A new measurement of J/ψ suppression in Pb-Pb collisions at 158 GeV per nucleon, *Eur. J. Phys. C* **39**, 335 (2005).
38. Rafelski, J., and Müller, B., *Phys. Rev. Lett.* **48**, 1066 (1982); **56**, 2334 (1986); Koch, P., Müller, B., and Rafelski, J., *Phys. Rep.* **142**, 167 (1986).
39. Georgi, H. M., *et al.*, *Ann. Phys. (NY)*, **114**, 273 (1978); Combridge, B. L., *Nucl. Phys.* **B151**, 429 (1979); Matsui, T., Svetitsky, B., and McLerran, L. D., *Phys. Rev. D* **34**, 783 (1986); **34**, 2047 (1986); **37**, 844 (1988).
40. Grayer, G., *et al.*, (1973). In *AIP Conf. Proc. 13* (AIP, New York).
41. Hamilton, R. P., *et al.*, *Phys. Rev. Lett.* **44**, 1182 (1980).
42. Wong, C.-Y. (1994). *Introduction to High-Energy Heavy Ion Collisions* (World Scientific, Singapore).
43. Eidelman, S., *et al.*, *Phys. Lett.* **B592**, 1 (2004).
44. Kapusta, J., and Mekjian, A., *Phys. Rev. D* **33**, 1304 (1986).

Bibliography

A reprint volume containing many of the pioneering papers on relativistic heavy ion collisions

Kapusta, J., Müller, B., and Rafelski, J. (2003). *Quark–Gluon Plasma: Theoretical Foundations* (Elsevier, Amsterdam).

Some books on the physics of relativistic heavy ion collisions

Csernai, L. P. (1994). *Introduction to Relativistic Heavy Ion Collisions* (Wiley and Sons, New York).

Wong, C.-Y. (1994). *Introduction to High-Energy Heavy Ion Collisions* (World Scientific, Singapore).

Letessier, J., and Rafelski, J., (2002). *Hadrons and Quark–Gluon Plasma* (Cambridge University Press, Cambridge).

Hwa, R., and Wang, X.-N. (eds.), (2003). *Quark–Gluon Plasma 3* (World Scientific, Singapore).

Shuryhak, E. V. (2004). *The QCD Vacuum, Hadrons and the Superdense Matter* (World Scientific, New Jersey).

A series of international conferences on the subject of relativistic heavy ion collisions:

Quark Matter 2002: The 16th Int. Conf. on Ultra-Relativistic Nucleus–Nucleus Collisions, Gutbrod, H., Aichelin, G., and Werner, K., (eds.), *Nucl. Phys.* **A715**, 3 (2003).

Quark Matter 2004: The 17th Int. Conf. on Ultra-Relativistic Nucleus–Nucleus Collisions, Ritter, H.-G. and Wang, X.-N. (eds.), *J. Phys. G* **30**, S633 (2004).